Chapter 6

Structural evolution, stability, and spectra of small silver and gold clusters: A view from the electron shell model

Pham Vu Nhat[a], **Nguyen Thanh Si**[a], **and Minh Tho Nguyen**[b]

[a]*Department of Chemistry, Can Tho University, Can Tho, Vietnam,* [b]*Institute for Computational Science and Technology (ICST), Quang Trung Software City, Ho Chi Minh City, Vietnam*

1. Introduction

Over the past decades, numerous studies, experimental and theoretical alike, have been devoted to the noble metal clusters owing to their special roles in photography, catalysis of chemical reactions, electronic materials, and medical treatments [1–5]. With a broad spectrum of antibacterial and antifungal activities, these systems are well suited for clinical and therapeutic applications [6,7]. More importantly, they are able to conjugate to a variety of bimolecular systems and much less toxic to human bodies in comparison to many other metallic compounds [8]. In addition, noble metal derivatives exhibit superior optical properties as compared with other transition metals and have therefore attracted a great deal of interest in the field of sensors, biosensors, and biomedical diagnostics [9–11]. It can be argued that both silver and gold clusters are among the most characterized atomic aggregates to date by both experimental techniques [12–15] and quantum mechanical calculations [1,16–20].

Identification of the most stable structures of elemental clusters has long been, and still is, a challenging but vital task in the field of cluster science, as it would provide us with deeper insights into many functional properties of this class of compounds [2]. Several research groups conducted extensive investigations to elucidate geometrical structures of silver/gold clusters [21–23]. The atomic arrangements of the small pure M_n (M = Ag, Au) clusters in the range of $n = 2$–20 and their growth pattern are now well characterized [24–29]. As a result of relativistic effects [30–32], the preference for planar shape of neutral gold clusters likely continues up to ~11 atoms [31]. Larger systems typically exist in hollow cages, and a structural transition from an oblate form to a pyramid-like shape is observed at Au_{17} [26]. Au_{20} has also been the focus of numerous studies, and a consensus, which was long reached, is that it prefers a T_d symmetry macro-tetrahedron characterized by a single peak infrared spectrum [25,26]. Although coinage metals share several analogies in their bulk states, their small clusters exhibit several differences in the gas phase, again as a result of relativistic effects [30,32]. For example, while gold clusters favor planar forms up to surprisingly large sizes, Cu clusters tend to adopt three-dimensional (3D) structures already at much smaller sizes [33]. Silver clusters are expected to behave in between, i.e., their 3D structures come out a little earlier than gold clusters, but later than copper counterparts.

Similar to alkali clusters, electron shell effects in silver and gold clusters are also operative since their n*d* states are completely occupied [34,35]. It has well been established that both Ag_n^+ and Au_n^+ cationic clusters exhibiting a high thermodynamic stability are found at $n = 3, 9, 21, 35, 41, 59, \ldots$, whereas the negatively charged counterparts are exceptionally abundant at $n = 7, 19, 33, 39, 57, \ldots$[36]. A widely accepted explanation for such a phenomenon is based on a strong delocalization of the external *s* electrons [37,38]. Accordingly, they can be treated as particles moving around a spherical pseudo-potential composed of the inner electrons along with the nuclei. This highly delocalized behavior of valence electrons brings about the main characteristics of simple metal clusters, including formation of electron shells and occurrence of shell closing effect that are somewhat similar to those in free atoms. Consequently, a cluster in which the number of valence electrons matches the shell closure, namely $1S^2/1P^6/1D^{10}/2S^2/1F^{14}/2P^6/\ldots$, is produced more abundantly as compared with the immediately preceding or following ones and is called a *magic* cluster. This approach, currently known as the phenomenological shell model (PSM), has been proven to be a simple but effective model to interpret the stability pattern and electronic structure of small-size metal clusters [39].

Atomic Clusters with Unusual Structure, Bonding and Reactivity. https://doi.org/10.1016/B978-0-12-822943-9.00020-6

In this chapter, we would review not only the structural evolution but also the stability trend of a series of small-sized silver and gold clusters M_n with $n = 2 - 20$. Geometric shapes of the lowest-energy structures and their basic thermodynamic parameters including the binding energy per atom, the second-order difference of energy, and the one-step fragmentation energy are determined and confirmed using density functional theory (DFT) computations. The electronic structure, which is at the origin of astonishing properties of clusters, is further elucidated within the perspective of the PSM. As such electronic distributions are well reflected in the excited states, their optical spectra are also analyzed to figure out the similarities and differences between two noble metal elements.

2. Equilibrium structures and growth mechanism

In the following sections, the possible equilibrium structures of silver and gold clusters, along with their growth mechanism, will be determined and confirmed. Conventionally, the structures presented hereafter are denoted as M_n-**X** in which M = Ag and Au, $n = 2$–20, and **X** = I, II… being isomers with increasing relative energy. Thus, M_n-**I** consistently stands for the most stable isomer of size n. For the sake of simplicity, relative energies are given hereafter in eV in single decimal figure.

The present review mostly discusses the computational results that were recently obtained making use of DFT approaches [22,26–28]. In our DFT computations, local energy minima are fully optimized, without any symmetry or geometry restrictions, employing a density functional with long-range-corrected exchange effects, namely the LC-BLYP functional [44], in conjunction with the effective core potential (ECP) cc-pVDZ-PP basis set [45]. This level of calculation has been tested earlier for quantitative examination of systems containing noble metals [28,46]. Harmonic vibrational frequency computations are also carried out at the same level to confirm the detected structures as local minima and to estimate their zero-point energy (ZPE) corrections.

With the aim to calibrate the performance of DFT methods, we first conduct some benchmark calculations for the dimers Au_2 and Ag_2 using various types of functionals along with the cc-pVDZ-PP basis set. Computed results are present in Table 1, which also includes available experimental data for the purpose of comparison. Generally, all functionals tested tend to overestimate the bond lengths of both Au_2 and Ag_2, except for the LC-BLYP. Deviations from experiment vary from 0.05 to 0.11 Å for Au_2 and from 0.03 to 0.13 Å for Ag_2 using traditional GGA and hybrid functionals. The LC-BLYP exhibits smallest deviations from experimental bond lengths with an error margin smaller than 0.03 Å (Table 1). This functional is also reliable in predicting vibrational frequencies. The LC-BLYP values $\omega_e(Au_2)$ and $\omega_e(Ag_2)$ amount to 190 and 203 cm^{-1}, respectively, which agree well with experimental values of 191 and 192 cm^{-1} [40,42].

Though the geometric and spectroscopic information can sufficiently be established by the LC-BLYP functional, it is likely to yield considerably inconsistent results for the bond dissociation energy (D_e). In fact, D_e values predicted by LC-BLYP/cc-pVDZ-PP computations for Au_2 and Ag_2 amount to 1.9 and 1.5 eV, respectively, which significantly underestimate the experimental values of 2.3 eV for Au_2 and 1.7 eV for Ag_2 [40,43]. GGA and meta-GGA functionals such as BP86, PW91, PBE, and TPSS produce better results for this quantity (Table 1). On the basis of a good agreement with the experiment for both Au_2 and Ag_2, the PBE functional appears to be more suitable for energetic quantities.

The above discussion clearly shows that it is rather difficult to judge the overall accuracy of a specific functional as each naturally has its own advantages and drawbacks, good performance, and shortcomings when treating a certain property. As discussed above, benchmark studies testing the accuracy of functionals were frequently performed on relatively small systems whose accurate experimental information or theoretical data from high-level MO calculations are available. Because most targets of actual interest have larger size and more complicated structure, the benchmarks do not always reflect the special structural or electronic features of medium and large-size compounds. Therefore, it is crucial for each case considered to carefully examine the applicability of different computational options for every new type of compounds. Although it is rather not wise to make a clear statement about the overall performance of a functional for both gold and silver clusters in all computations, the LC-BLYP appears reliable in predicting molecular geometries and vibrational signatures, but it is likely to be deficient in computing the bond energy for which the PBE seems to describe a bit better. For the TPSSh and M06-L functionals, results in Table 1 show that they are not more reliable than the LC-BLYP in predicting atomic geometries and vibrational signatures and also not better than the PBE in determining the bond energies. Therefore, we select both LC-BLYP and PBE functionals for most calculations carried out in this report. While the former is employed for prediction of the lowest-energy structures, the latter is used for determination of energetic parameters.

Both silver and gold clusters prefer planar structure up to $n = 6$ in their ground state (Fig. 1). The M_2 dimers have a low spin (singlet) ground state with bond lengths of 2.50 (Au_2) and 2.53 Å (Ag_2) at the LC-BLYP/cc-pVDZ-PP level. These are closely comparable to the experimental values of 2.47 Å (Au_2) [40] and 2.53 Å (Ag_2) [41]. The M_3 trimers adopt a bent structure, which is distorted from a Jahn-Teller effect on a D_{3h} form. A single occupancy of the doubly degenerate e orbital

TABLE 1 Theoretical and experimental bond lengths (R, Å), vibrational frequencies (ω_e, cm^{-1}), and dissociation energies (D_e, eV) of dimeric Au_2 and Ag_2 species.

	Au_2			Ag_2		
DFT functional	R_e	ω_e	D_e	R_e	ω_e	D_e
B3LYP	2.56	167	1.94	2.59	179	1.56
B3P86	2.52	176	2.08	2.56	190	1.63
PW91	2.53	173	2.28	2.56	188	1.81
BB95	2.53	171	2.25	2.57	187	1.81
B3PW91	2.53	174	1.97	2.57	186	1.51
BP86	2.53	173	2.23	2.56	188	1.78
BPW91	2.54	171	2.13	2.57	186	1.66
M06	2.58	162	2.14	2.59	192	1.83
M06-2X	2.56	159	1.49	2.68	154	1.40
M06-L	2.56	160	2.26	2.57	189	1.90
PBE	2.53	172	2.27	2.57	186	1.78
PBE0	2.53	175	2.00	2.57	185	1.55
TPSS	2.52	176	2.25	2.56	191	1.76
TPSSh	2.52	177	2.15	2.56	190	1.67
LC-BLYP	2.50	190	1.88	2.53	203	1.46
Experiment	2.47[a]	191[a]	2.29[a]	2.53[b]	192[c]	1.66[d]

[a]*Taken from Ref. [40].*
[b]*Taken from Ref. [41].*
[c]*Taken from Ref. [42].*
[d]*Taken from Ref. [43].*

of the equidistant triangle (D_{3h}) leads to a geometric distortion giving rise to an orbital splitting to a pair of ($a_1 + b_2$) orbitals (Fig. 2) in the C_{2v} form. The unpaired electron in both Au_3 and Ag_3 tends to occupy the b_2 SOMO, resulting in a $^2B_2$ ground state.

A planar rhombus having a D_{2h} point group is predicted to be most stable form of the tetramers M_4. Starting from the square D_{4h} cycle with a singlet $^1A_{1g}$ state, a Jahn-Teller vibrational deformation following a normal mode, being a simultaneous ring deformation mode B_{1g}, leads to a substantially stabilized rhombic D_{2h} structure. The M_4 species with D_{4h} structure would have had two electrons in a degenerate e_u orbital (Fig. 3). Such a degenerate state is not stable upon Jahn-Teller distortions, and the system undergoes a geometry relaxation to remove that degeneracy. The resulting stable structure of M_4 is thus distorted from D_{4h} to D_{2h} with a low spin ^1A_g state. Let us note that a Y-shaped isomer of Au_4, not shown in Fig. 1, is calculated to have a similar energy content to the rhombic one.

In agreement with previous predictions, the global minima of Au_5 and Au_6 are a planar W-type shape (C_{2v}) and a planar triangle (D_{3h}), respectively. Generally, the equilibrium geometry of a specific system M_n in the size range of $n = 2$–6 is generated by simply adding an extra M atom to the lowest-lying isomers of the smaller-size M_{n-1}.

The lowest-energy structures and isomers for M_n from $n = 7$ to 11 clusters are shown in Fig. 4. The most stable form Au_7-**I** is reached from Au_6-**I** by adding an extra Au atom, followed by a 3D configuration Au_7-**II**. The 3D structure has a higher symmetry (C_{2v}) but is less stable than Au_7-**I** by 0.2 eV. As in Au_7, the planar shape Au_8-**I** (D_{2h}) is predicted as the global minimum of Au_8, whereas the second most stable isomer Au_8-**II** has a 3D conformation (T_d), being 0.7 eV higher. The planar D_{2h} structure was also reported as the lowest-energy isomer when CCSD(T) computations with the correlation consistent basis sets were employed [47].

The most stable form Au_9-**I** of Au_9 has again a planar arrangement and is generated by attaching one extra gold atom to the most stable isomer of Au_8-**I**. The next isomer Au_9-**II** is computed to be about ~0.1 eV higher. Previous DFT calculations

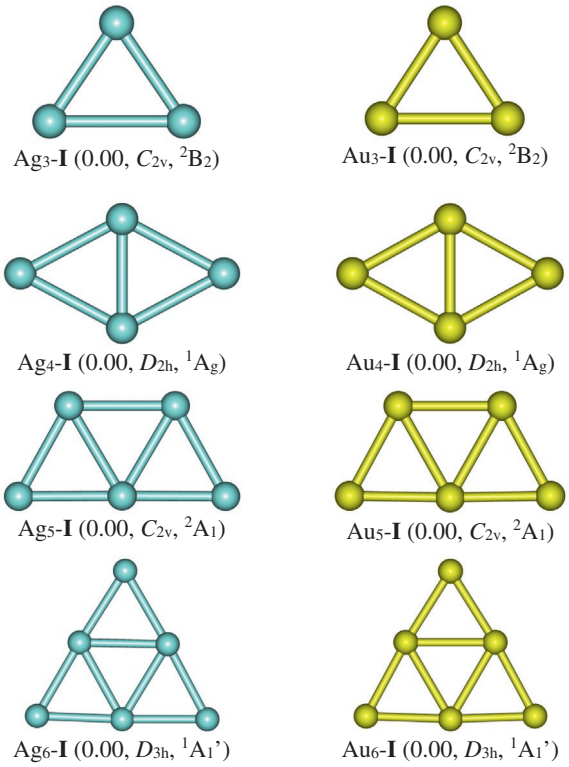

FIG. 1 The lowest-energy isomers for M_n clusters, M = Ag, Au, $n = 3$–6.

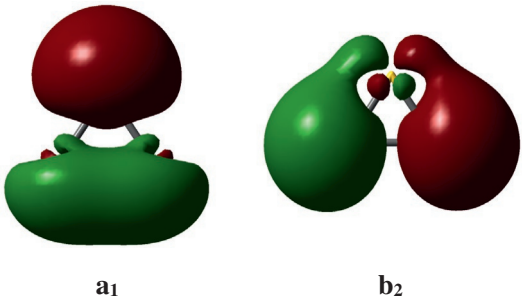

FIG. 2 Plots of the a_1 and b_2 orbitals in the C_{2v} M_3 clusters.

[48,49] also reported Au_8-**I** and Au_9-**I** as the best candidates for equilibrium geometries. In the case of Au_{10}, the 3D structure Au_{10}-**I** (Fig. 4) is predicted to be preferred over the planar elongated hexagon Au_{10}-**II**, with an energy of ~0.2 eV (LC-BLYP value).

As mentioned above, the 2D → 3D transition in neutral Au_n is still a matter of debate as it remains sensitive to the computational method employed. Some previous investigations recorded a crossover already at $n = 7$ [33], while other studies predicted it to occur somewhere between $n = 12$ and 15 [24]. Our present geometrical search points out that such a transition from planarity to nonplanarity is likely to be initiated at $n = 10$, and Au_{10} represents the first size whose lower-lying structures do not have a 2D shape. This is consistent with a recent investigation [48] in which this transition is predicted to start from Au_{10}. The 3D Au_{11}-**I** is confirmed in agreement with previous reports [48,49]. This global minimum contains a trigonal prism as the main structural feature and lies ~0.5 eV lower in energy than the planar Au_{11}-**II**.

In contrast to the propensity of small gold clusters to favor a planar conformation, densely packed 3D structures tend to dominate the lower-lying population of silver Ag_n clusters with $n > 6$. Indeed, two 3D configurations, namely a D_{5h} pentagonal bipyramid Ag_7-**I** and a C_{3v} tricapped tetrahedron Ag_7-**II**, are competing for the lowest-lying equilibrium geometry of Ag_7. Similar to earlier results [18,22,50], the former is the most stable isomer. For Ag_8, the T_d Ag_8-**I** arising from a regular tetrahedron capped with four Ag atoms is predicted to lie ~0.3 eV higher in energy than a D_{2d} geometrical shape

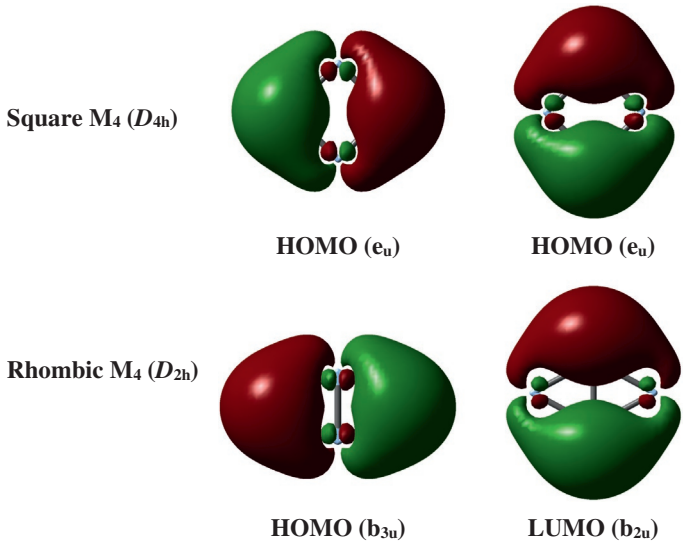

FIG. 3 Degenerate HOMOs in a square M_4, and their counterparts in a rhombic M_4.

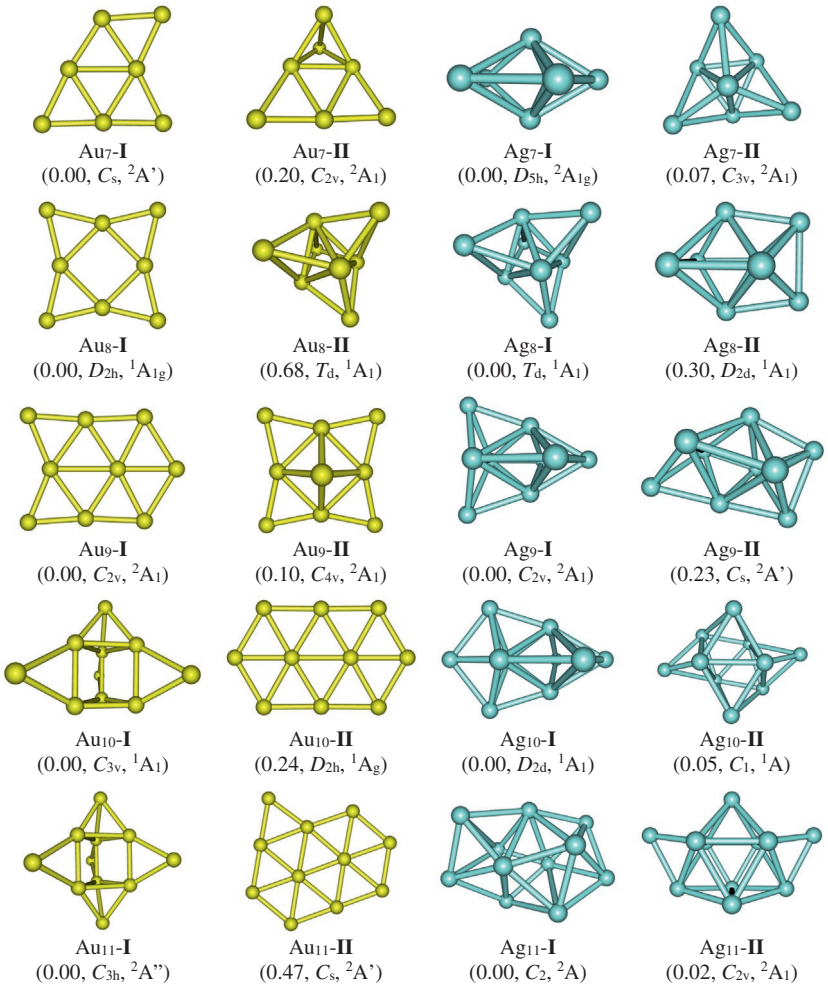

FIG. 4 Lower-energy isomers of M_n from $n=7$ to 11 clusters.

Ag_8-**II** (LC-BLYP/cc-pVDZ-PP). Our current prediction for the most stable isomers of both Ag_7 and Ag_8 is again in line with most previous calculations [2,51–53].

Consistent with earlier DFT calculations [52,54,55], the most stable isomer of Ag_9, i.e., Ag_9-**I** with C_{2v} symmetry, is formed by adding one Ag atom to the T_d Ag_8-**I**. However, this form was considered as a local minimum in some other studies [18,56]. The Ag_9-**I** is computed to be ~0.2 eV more stable than Ag_9-**II** (LC-BLYP value). In going further, Ag_{10} is created by adding one extra silver atom to the most stable D_{2d} isomer of Ag_9. Such a twinned pentagonal bipyramid has also been considered to be the ground state by Fournier [16] and Yang et al [55]. The next most stable isomer Ag_{10}-**II** is higher than Ag_{10}-**I** by only 0.05 eV in energy (LC-BLYP value). This asymmetric form has also been suggested to be the lowest-energy structure of Ag_{10} in some other previous reports [50,56].

For Ag_{11}, two nearly degenerate isomers within 0.02 eV energy range are competing for the ground state. The C_2 Ag_{11}-**I** was reported as a local minimum in earlier studies [50,56], but the C_{2v} Ag_{11}-**II** has recently been considered to be the best candidate for the ground state of Ag_{11} [22]. Overall, starting from the size $n=6$, both silver and gold clusters grow in completely different patterns. Some lower-lying isomers for M_n systems from $n=12$ to 16 are displayed in Fig. 5. Accordingly, both Au_{12} and Au_{13} exhibit 3D ground state. Flat structures are also found for these sizes but only as high-energy isomers. At the level of theory used, 2D conformations Au_{12}-**II** and Au_{13}-**II** are ~0.2 eV higher than their 3D counterpart. The results obtained here thus disagree with BLYP calculations reported in ref. [57] in which the equilibrium geometries of both Au_{12} and Au_{13} are planar forms, namely Au_{12}-**II** and Au_{13}-**II**, respectively. The two most stable isomers detected for Au_{14}, i.e., Au_{14}-**I** and Au_{14}-**II**, are all 3D (Fig. 5). Similarly, the nonplanar-shape Au_{15}-**I** is reached by capping an extra Au atom upon one side of Au_{14}-**I**. The second most stable Au_{15}-**II** is only ~0.2 eV higher. The structures Au_{14}-**I** and Au_{15}-**II** located here were also previously suggested as the global minima for Au_{14} and Au_{15}, respectively [49,57–59]. In accordance with earlier reports [26,50], the T_d Au_{16}-**I** is predicted to be ~0.1 eV lower than the C_s Au_{16}-**II**.

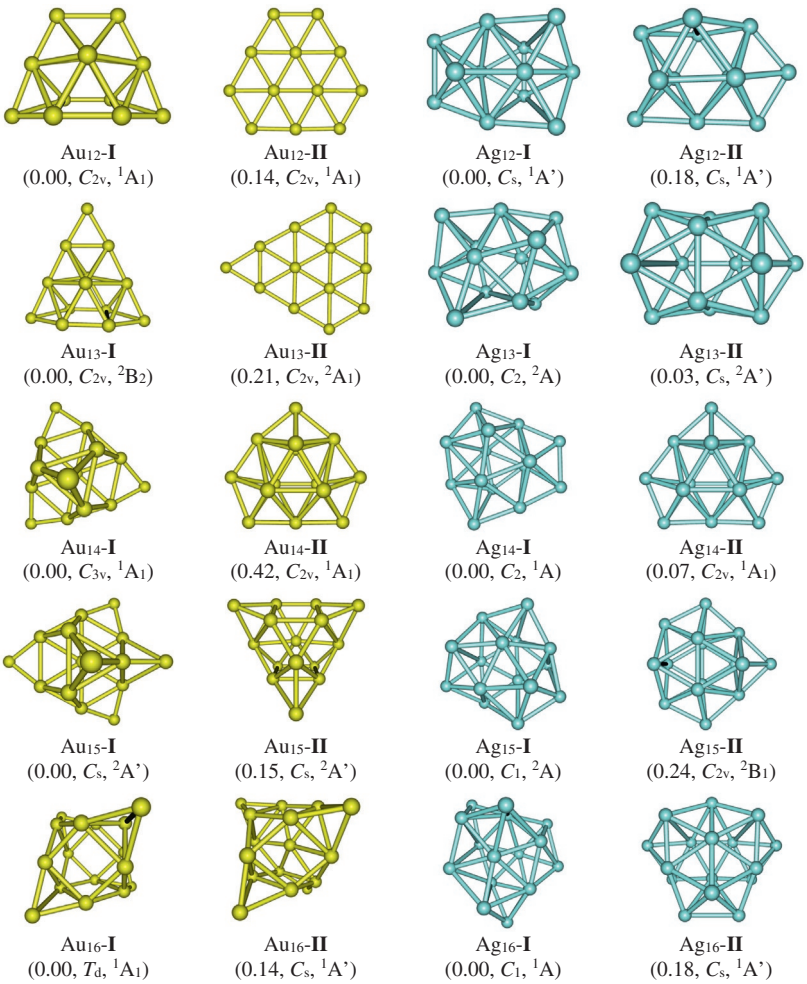

FIG. 5 Lower-energy isomers of M_n clusters from $n=12$ to 16.

For silver counterparts, the lowest-lying Ag_{12}-**I** has a C_s symmetry and can be derived from Ag_{11}-**I**. The next most stable Ag_{12}-**II** also has C_s symmetry and lies ~0.2 eV higher. In agreement with a recent report [18], the most stable Ag_{13}-**I** is obtained by capping one Ag atom on an edge of Ag_{12}-**I**. The next isomer Ag_{13}-**II**, which was suggested to be the most stable structure by Yang et al. [55], is computed to be only 0.03 eV less stable than Ag_{13}-**I** in our current work. Both forms are thus quasidegenerate isomers.

The C_2 Ag_{14}-**I**, reached by capping one Ag atom to Ag_{13}-**I**, is recently computed to be the lowest-energy Ag_{14} [22]. The next most stable structure, i.e., Ag_{14}-**II**, is somewhat more symmetric (C_{2v}) and lies only 0.1 eV higher (LC-BLYP value). From attachment of one silver atom Ag_{14}-**I** and Ag_{14}-**II**, two lowest-lying isomers Ag_{15}-**I** (C_1) and Ag_{15}-**II** (C_{2v}) are built upon. They possess a substantial energy gap, in which the former is ~0.2 eV below the latter. This result is inconsistent with recent calculations by Rodríguez-Kessler et al. [60] in which Ag_{15}-**II** was predicted as the global minimum, whereas Ag_{15}-**I** has not been seen. Accordingly, the low symmetry Ag_{15}-**I** emerges as the new global minimum not detected before [61]. In agreement with this report [60], two oblate configurations Ag_{16}-**I** and Ag_{16}-**II** with an energy difference of ~0.2 eV (LC-BLYP value) are the most stable forms of Ag_{16}. Again, the growth patterns of the two series of noble metal clusters differ much from each other and do not induce any correlation.

We now examine the lower-lying structures of systems having 17–20 metal atoms that are shown in Fig. 6. Previously, the asymmetric Au_{17}-**II**, which can be considered as a result of removal of three atoms on one edge of the tetrahedral Au_{20} cluster, was reported to be the lowest-energy Au_{17} [49]. However, our current LC-BLYP results point out that this size prefers to exist in the highly symmetric T_d Au_{17}-**I** form. Following attachment of one gold atom to Au_{17}-**II**, the lowest-energy Au_{18}-**I** of the octadecamer Au_{18} is built upon. The next low-lying structure Au_{18}-**II** is computed to stay ~0.1 eV higher. Continuously, the most stable forms of Au_{19} and Au_{20}, i.e., Au_{19}-**I** and Au_{20}-**I** in Fig. 4, are obtained from Au_{18}-**I** upon addition of one and two Au atoms. The regularly tetrahedral pyramid Au_{20}-**I** and the truncated pyramid Au_{19}-**I** have also unambiguously been assigned as the global energy minima for both Au_{20} and Au_{19} systems, respectively [25,62].

Competitive candidates with tiny energy gaps have been found for systems containing from 17 to 20 silver atoms [22,50]. Two foremost lower-lying isomers of Ag_{17} are the close-packed structure Ag_{17}-**I** and the hollow cage Ag_{17}-**II** (Fig. 6). Ag_{17}-I turns out to be a new structural motif, which was not found in previous studies. At the LC-BLYP/cc-pVDZ-PP level, the former is computed to be ~0.2 eV higher in energy than the latter. Similarly, several configurations

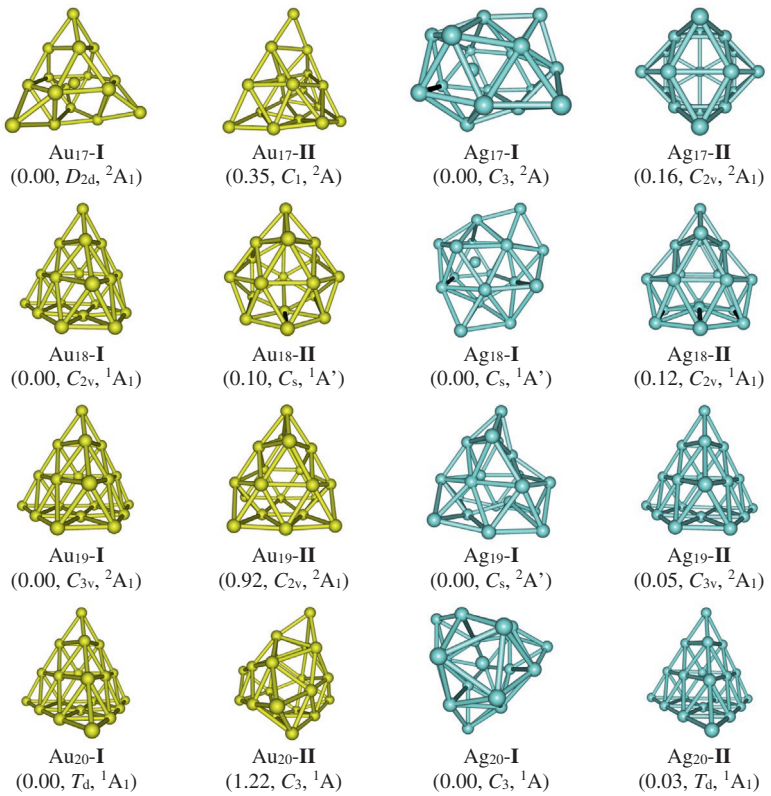

FIG. 6 Lower-energy isomers for M_n clusters with n from 17 to 20.

also exist in competing for the ground state of Ag_{18}. Consistent with a recent study [18], a derivative of the Ag_{13} icosahedron with C_s symmetry, i.e., Ag_{18}-**I** in Fig. 6, is detected as the ground-state geometry of Ag_{18}. The C_{2v} hollow cage Ag_{18}-**II**, which was considered as the best candidate for the global minimum in ref. [50], is now computed to lie ~0.1 eV above.

For Ag_{19}, while Tsuneda [28] suggested a pyramid motif, i.e., the truncated trigonal pyramid Ag_{19}-**II** (C_{3v}), to be the lowest-energy structure, we identify this form to be marginally less stable by 0.05 eV than the C_s isomer Ag_{19}-**I**. Similarly, the pyramidal motif Ag_{20}-**II** was located as the most preferred structure of Ag_{20} in several reports [18,50,54]. However, the newly detected eicosamer Ag_{20}-**I**, having a C_3 symmetry, is computed to be only 0.03 eV more stable than Ag_{20}-**II** (LC-BLYP value) [22,39].

Based on computational results reported in recent literature for small M_n clusters [22,60] and combined with our present calculations, structural evolutions in going from M_3 to M_{20} are summarized in Figs. 7 and 8. Overall, the preference of a *successive growth pattern* in gold clusters is not as much recognizable as in silver counterparts. Particularly, in the size range of Ag_{12}–Ag_{16}, the most stable form of a specific size n can regularly be obtained upon addition of an extra Ag atom to the lowest-lying isomer of the smaller $n-1$ size. Such an evolution, which forms the basis for the successive growth algorithm for structural search, can be employed to predict the favored structures of silver clusters. Nevertheless, such a pattern is broken at a certain size where a completely different structural feature emerges. It is, for example, the case of Ag_{17} whose corresponding global minimum is not derived from the most stable Ag_{16}. It could arise from a higher energy isomer of a smaller size but the reasons for such a strong stabilization are not clear.

In summary, while Ag_n clusters prefer a planar structure up to $n=6$, a structural transition from 2D to 3D in gold systems is likely to take place at Au_{10}. From $n=7$, Ag_n species and their Au_n counterparts exhibit much different ground-state geometries. The Ag_n clusters going from $n=7$ to 11 adopt three-dimensional structures that can be constructed following a successive growth algorithm, that is, by adding extra Ag atoms either on the D_{5h} bipyramid Ag_7-**I** or the T_d tetrahedral Ag_8-**I**. For systems from $n=13$ to 16, hollow flat cages become the most favored configurations. As the cluster size increases, a common trend emerges for formation of close-packed structures from a 13-atom icosahedral core by adding extra atoms on the triangular faces. As compared with the silver Ag_n, the gold Au_n clusters generally exhibit more highly symmetric ground-state structures. The local minima of a specific Au_n system are usually generated from the lowest-lying isomer of the smaller-size Au_{n-1} by adding an extra gold atom around. Remarkably, in contrast to a preference of amorphous structures obtained for silver clusters, the pyramid-like motif is the most energetically favorable structure in Au_n systems with $n=18$–20. This can be understood by the fact that the contribution of *d* electrons in the small silver clusters is more significant than in gold counterparts [63]. On the one hand, the effects of *d* electrons and *s*–*d* hybridization strongly

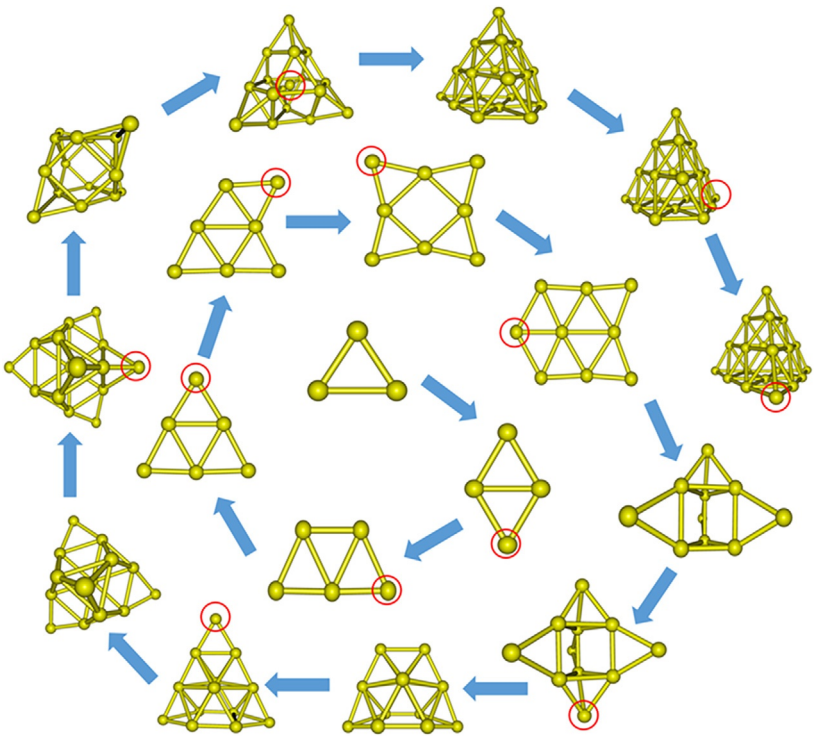

FIG. 7 Structural evolution from Au_3 to Au_{20} clusters. The added Au atom is labeled as ○ in *red* (*dark gray* in print version). *(Results are taken from P.V. Nhat, N.T. Si, J. Leszczynski, M.T. Nguyen, Another look at structure of gold clusters Au_n from perspective of phenomenological shell model, Chem. Phys. 493 (2017) 140–148 and present work.)*

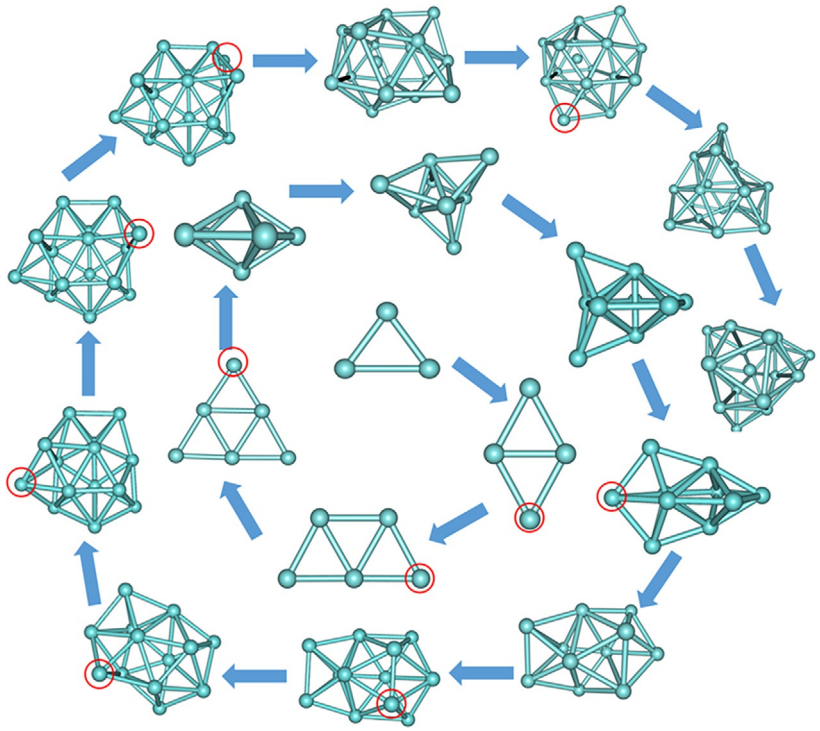

FIG. 8 Structural evolution from Ag_3 to Ag_{20} clusters. The added Ag atoms is labeled as ○ in *red* (*dark gray* in print version). *(Results are taken from P.L. Rodríguez-Kessler, A.R. Rodríguez-Domínguez, D.M. Carey, A. Muñoz-Castro, Structural characterization, reactivity, and vibrational properties of silver clusters: a new global minimum for Ag_{16}, Phys. Chem. Chem. Phys. 22 (46) (2020) 27255–27262, M.L. McKee, A. Samokhvalov, Density functional study of neutral and charged silver clusters Ag_n with n = 2–22. Evolution of properties and structure, J. Phys. Chem. A 121 (26) (2017) 5018–5028 and present work.)*

influence the ground-state configuration of silver clusters. On the other hand, the relativistic effects that are very important in heavier atoms such as gold [33] play a vital role in stabilizing the pyramidal structures.

3. Thermodynamic stabilities

To gain some quantitative insights into the thermodynamic stabilities of these neutral noble metal clusters, we now evaluate the change of binding energy per atom (*BE*), the second-order difference of energy ($\Delta^2 E$), and the one-step fragmentation energy (E_f) with respect to the cluster sizes. For these clusters, such parameters of a specific system M_n (M = Ag, Au) are defined by following equations:

$$BE = [nE(\mathrm{M}) - E(\mathrm{M}_n)]/n$$

$$\Delta^2 E = [E(\mathrm{M}_{n+1}) + E(\mathrm{M}_{n-1}) - 2E(\mathrm{M}_n)]$$

$$E_f = E(\mathrm{M}_{n-1}) + E(\mathrm{M}) - E(\mathrm{M}_n)$$

where $E(M_n)$ is the total energy of the lowest-lying M_n cluster shown above.

The graph illustrating the variation of BE as a function of gold cluster size is plotted in Fig. 9. This parameter can be regarded as the energy gained in assembling a definite cluster from isolated gold constituents. Previously, a theoretical study [64] employed a local density approximation (LDA) to calculate the E_b of gold clusters up to Au_{20}, but experimental data are not systematically reported yet. Our present results are quantitatively different from earlier values [61]. As shown in Fig. 9, the BE plot of Au_n clusters roughly exhibits a gradual growth and reaches the maximal value of 2.3 eV/atom for Au_{20}. This is still much smaller than the cohesive energy of 3.8 eV obtained for the bulk gold [65]. In addition, computed results show local maxima at $n = 6$, 8, and 20, suggesting that these clusters are expected to be more stable than their immediate neighboring ones.

The value $E_f = 2.3$ eV obtained for Au_2 (at PBE/cc-pVDZ-PP level) is in line with the experimental value of 2.29 ± 0.02 eV [40]. Generally, calculated E_f values as a function of cluster size obey an odd-even oscillation. Accordingly, clusters with an even number of atoms appear to be more stable than the neighboring odd-numbered ones. Of these clusters, Au_3 and Au_7 are characterized by the lowest E_f values, implying their low thermodynamic stability. On the contrary, Au_6 and Au_{20} are expected to be the most stable ones as they exhibit exceptionally high E_f values. Other remarkably high peaks are found at $n = 2$, 8, 12, and 14, indicating that these systems are also particularly stabilized.

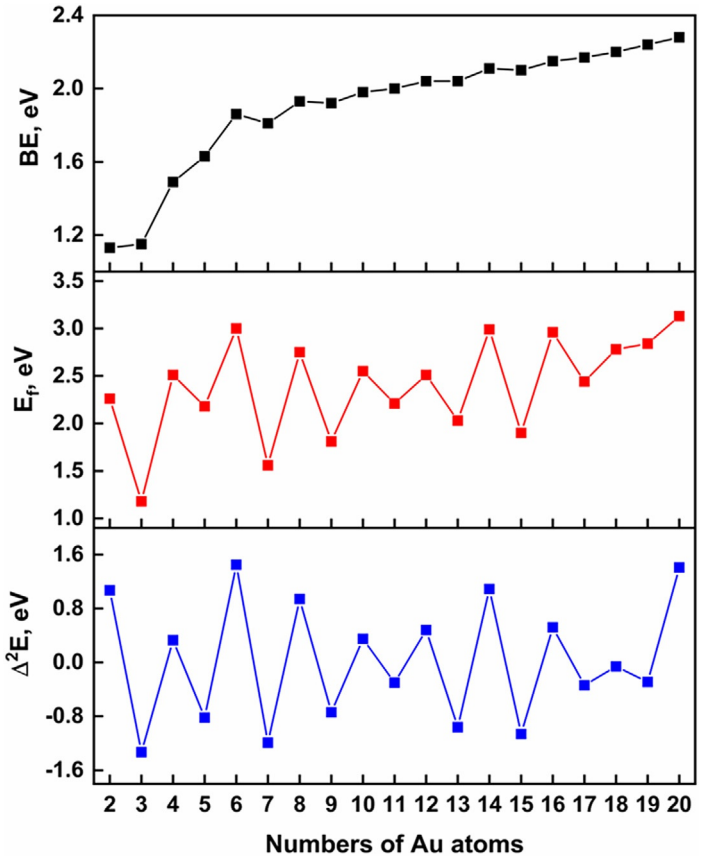

FIG. 9 Binding energies per atom (E_b), one-step fragmentation energies (E_f), and second-order difference of energy ($\Delta^2 E$) for neutral Au_n clusters as a function of cluster size. Results are obtained at the PBE/cc-pVDZ-PP+ZPE level.

As discussed above, the optimal structure of Au_n at a certain size is normally generated from that of the smaller one by adding an extra gold atom. Accordingly, the energy gain in incorporating an Au to the smaller size can be considered as the embedding energy (*EE*). Such a parameter can also be characterized by the one-step fragmentation energy (E_f), i.e., the energy needed to detach one gold atom from Au_n, giving rise to Au_{n-1}. Evolution of the E_f values for the Au_n clusters considered, calculated at the PBE/cc-pVDZ-PP+ZPE level, is also plotted in Fig. 9.

The second-order difference of energy ($\Delta^2 E$) is an important indicator that measures the relative stability of clusters. In particular, peaks in the graph of $\Delta^2 E$ as a function of cluster sizes were found to be well correlated with peaks in the experimental mass spectra [66]. As illustrated in Fig. 9, an extreme odd-even oscillation appears indicating that a cluster having an even number of atoms is more stable than the odd-numbered ones. Consistent with the above analyses based on fragmentation energies, the Au_6 and Au_{20} species are found to have the largest $\Delta^2 E$ values, indicating their peculiarly high thermodynamic stability. On the contrary, the Au_3 and Au_7 systems are again found to be the least stable sizes.

Concerning the relative stability of silver clusters, different density functionals have been employed to predict the total atomization energies of Ag_n clusters up to $n=99$ [18]. Accordingly, the closed-shell systems having an even number of silver atoms were generally found to be more stable than the open-shell counterparts exhibiting an odd number of electrons. In addition, total atomization energies of Ag_n start converging slowly to the bulk at the size $n=55$ and reach the maximal value of 2.2 eV/atom for Ag_{99}. Our computed atomization energy or the binding energy per atom as function of Ag_n size up to $n=20$ is displayed in Fig. 10. As in gold systems, the E_b of Ag_n species also increases slowly with the cluster size and reaches the maximum of 1.9 eV/atom at $n=20$. This is again much smaller than the cohesive energy of 2.9 eV of bulk silver [18].

The energetics for detachment of an Ag atom from a cluster Ag_n to form a smaller species Ag_{n-1} up to $n=20$ are also illustrated in Fig. 10. At the PBE/cc-pVDZ-PP level, the fragmentation energy (E_f) of Ag_2 amounts to 1.8 eV, which is comparable to the experimental value of 1.7 eV [43]. Such a result in addition suggests that the chemical bond in a silver cluster is more breakable than that of the gold counterpart. The largest fragmentation energy for Ag_{20} (~2.7 eV) is ~90% of 2.9 eV for bulk silver [18]. Similar to gold clusters, an even-odd oscillation appears in the calculated E_f values as a function of Ag_n size (Fig. 10), in which even-numbered systems are thermodynamically more stable than odd-numbered ones. Of the

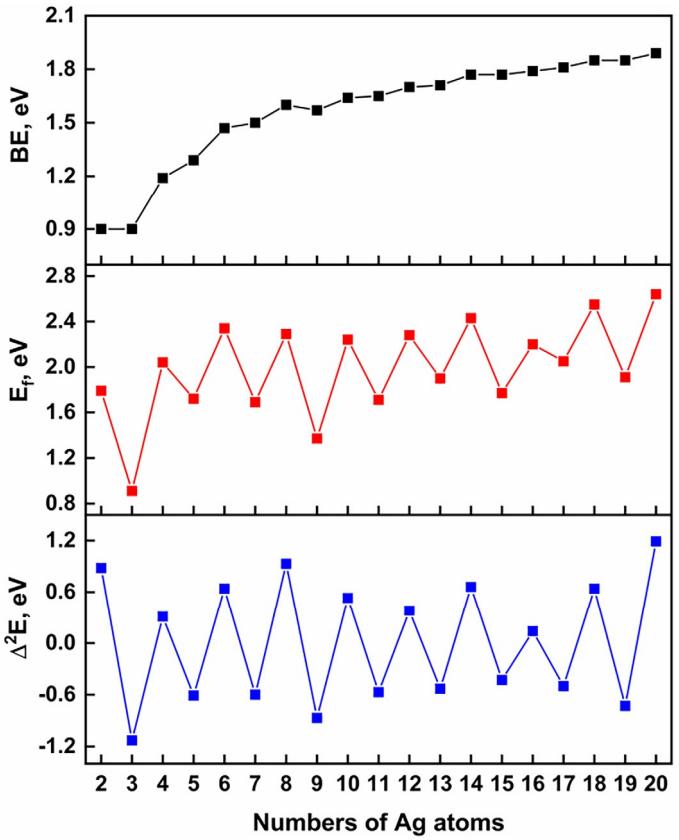

FIG. 10 Binding energies per atom (E_b), one-step fragmentation energies (E_f), and second-order difference of energy ($\Delta^2 E$) for neutral Ag_n clusters as a function of cluster size. Results are obtained at the PBE/cc-pVDZ-PP+ZPE level.

clusters considered, Ag_3 and Ag_9 are predicted to be the least stable species, being characterized by the lowest E_f values. In contrast, Ag_6, Ag_8 Ag_{14}, and Ag_{18} are expected to be particularly stable as their E_f values are exceptionally high.

The even-odd fluctuation becomes more obvious when we look at the second-order difference of energy ($\Delta^2 E$). This thermodynamic parameter can also be considered as a disproportionation energy, being the energy change of such reaction

$$2Ag_n \rightarrow Ag_{n+1} + Ag_{n-1} \quad (1)$$

In agreement with the analysis based on dissociation energies given above, the Ag_6, Ag_8, and Ag_{14} species are found to be particularly stable with sharply high $\Delta^2 E$ values. Fig. 10 also reveals that while the disproportion of even Ag_n clusters is endothermic, that of odd counterparts is generally exothermic. Furthermore, the energy difference tends to decrease as the cluster size increases. For instance, the energies of reactions (1) are calculated to be ~0.8 and ~0.5 eV for $n=6$ and 12, respectively.

Two factors that determine the metal cluster stability include the electron shell effect and atomic arrangement [67]. Similarly to alkali clusters, the former can also be observed in clusters of coinage metals, because the n*d* levels of these elements are (almost) completely occupied [34,35]. However, a particular attention should be paid to the behavior of their *d* electrons. The participation in bonding of these fermions can be seen experimentally via cohesive energy of the bulk materials. For example, the experimental cohesive energy of Sc amounts to 3.9 eV/atom, then it increases to 4.9 eV/atom for Ti and attains a maximum value of 5.3 eV/atom for V. After this maximum, it decreases, reaching a bottom for Mn (2.9 eV/atom), then increases, having a broad maximum (4.3–4.4 eV/atom) for Fe, Co, and Ni, and finally, it decreases again, approaching another valley (3.5 eV/atom) at Cu [68]. Morse [40] pointed out earlier that the 4*s* orbitals of the first transition metal series have more significant contribution to the chemical bonding than the 3*d* orbitals because the latter are more contracted. Moving down in the Periodic Table, while the *d* orbitals tend to expand, the *s* orbitals are getting contracted [69]. Hence, the n*d* and (n+1)*s* orbitals of the second and third transition metal series become nearly comparable in size, thereby facilitating the *d* bonding. This may result in a greater stabilization of compounds containing heavier transition metals, as compared with those of the first-row metal elements, even though such a correlation remains not linear. In fact, the bond dissociation energies of V_2 and Nb_2 are determined to be 2.75 ± 0.01 [70] and 6.20 ± 0.05 eV [71], respectively, while that of Ta_2 is predicted to be in the range from 5.0 to 5.4 eV [72].

For gold-containing compounds, it should be noted that another crucial factor making their properties unique is the relativistic effect [49], rather than the "*lanthanoid contraction*" as mentioned above. Actually, the relativistic maximum of gold, which was initially pointed out by Pyykkö [30], results in many unusual molecular shapes and properties of gold compounds. In fact, while the ground state of Ag_7 has a 3D structure, that of Au_7 is planar, separated from the optimal 3D isomer by 0.2 eV (LC-BLYP value). The propensity of neutral gold clusters to favor planar structures continues up to surprisingly large sizes, being likely up to 10 atoms (see above). The strong relativistic effects in addition enhance the *d–d* interaction, leading to a stabilization of Au—Au bond [73,74]. As a result, the gold-gold distance in metal is getting even shorter than the corresponding silver-silver distance, being 2.88 and 2.89 Å, respectively [75]. A similar phenomenon also appears in dimers in which the bond dissociation energy of Au_2 (2.29 ± 0.02 eV) is significantly larger than that of Ag_2 (1.65 ± 0.03 eV) [40]. Without relativistic effects, interactions between fulfilled *d* orbitals become negligible; the bond strength between gold atoms could thereby be weaker than that between silver counterparts, because the *s* orbital shrinks down in the group. Also owing to strong relativistic effects, Au(I) compounds tend to aggregate (polymerize) via formation of weak gold-gold bonds with a length of ~3.0 Å and a strength of ~7–12 kcal mol^{-1}, a phenomenon known by the terms of *aurophilicity* or *aurophilic attraction* [76].

4. Phenomenological shell model (PSM)

As demonstrated above, not only the geometrical and electronic structure but also the (physical and chemical) properties of atomic clusters strongly depend on their size and differ considerably from both individual atoms and bulk materials [66,77]. Experimental observations become more and more available owing to the use of modern spectrometric techniques, and theoretical steps can be taken for understanding and elucidating the observed findings. However, similar to the situation in other fields, it is not always straightforward to understand experimental or calculated results, which often need to be rationalized with the help of some simpler approaches. In this context, the PSM [78] provides us with a simple but effective model to interpret the electronic structure and stability pattern of simple metal clusters [39].

In the original formulation of PSM, the shape of stable clusters is presumed to be spherical. The highly delocalized valence electrons that play a central role in the formation of chemical bonding in clusters are treated as itinerant particles moving around a spherical pseudo-potential composed of the inner electrons along with the nuclei, giving rise to the spherical shell closures, namely 1S/1P/1D/2S/1F/2P. Subsequently, the model was extended to treat elliptical shapes, known as the Clemenger-Nilsson model (CNM) [79], which was introduced to account for both spherical and oblate/prolate clusters, and from which the energy ordering of different levels with respect to the distortion of the cluster shape is qualitatively shown in Fig. 11.

As well established in the earlier literature [78,80,81], alkali clusters bearing 8, 18, 20, 40, 58, and 92 valence electrons exhibit an outstanding thermodynamic stability. A widely accepted explanation for such a phenomenon is based on a strong delocalization of the external *s* electrons bound in a spherically symmetric potential well [37,38]. Noble metal systems related to closed valence shell with $1S^2/1P^6/1D^{10}/2S^2$ electronic configurations have also been found to show particularly low polarizabilities, high ionization energies, and large dissociation energies [22]. These observations indicate the dominant contribution to formation of chemical bonding of 5*s* (Ag) and 6*s* (Au) electrons, reproducing the comparable closed electron shell numbers of the alkali clusters. Hence, to some extent, the electron distribution of silver clusters can be considered as similar to those of the alkalis. The M_n species with $n = 6$, 8, 20 considered in the present work provide us with some interesting samples for applications of the PSM. We now examine the electronic structure of some spherical systems based on a perspective of the PSM.

A cluster would exhibit a nearly spherical shape when all 3 P or all 5 D shell orbitals are filled with 6 or 10 electrons, respectively, in order to form a closed electronic structure (Fig. 11). As presented in Fig. 1, the lowest-energy structure of both Au_6 and Ag_6 is an equivalent triangle with a D_{3h} point group. This form was also reported as the ground-state geometry of Cu_6 [82]. The number of itinerant electrons amounts to six (one electron from each coinage metal atom) that formally satisfy the Hückel $(4n+2)$ counting rule for planar aromatic compounds. The clusters are characterized by planar shape; hence, an $1S^2\{1P_x^2 1P_y^2\}$ electronic configuration is expected (the curly brackets represent a double degeneracy). The energetic ordering of the valence molecular orbitals shown in Fig. 12 clearly approves the fact that the cluster with six itinerant electrons exhibits a $1S^2$ $\{1P_x^2 1P_y^2\}$ configuration. The two higher-lying orbitals, i.e., the degenerate HOMO, show an *p*-character, whereas the HOMO-1 is actually an *s*-orbital. Earlier, the electronic mechanism of how the Au_6 ring encapsulates a transition metal dopant atom was also successfully interpreted using such a simple model [83].

As mentioned above, irrespective of some similarities in bulk states, coinage metal clusters exhibit several significant differences in terms of geometrical shapes. For Ag_8, the 3D T_d structure (Fig. 4) is located as the ground-state geometry, and so is for Cu_8 [82]. On the contrary, Au_8 prefers the D_{2h} planar shape, being more stable than the T_d conformation by 0.7 eV

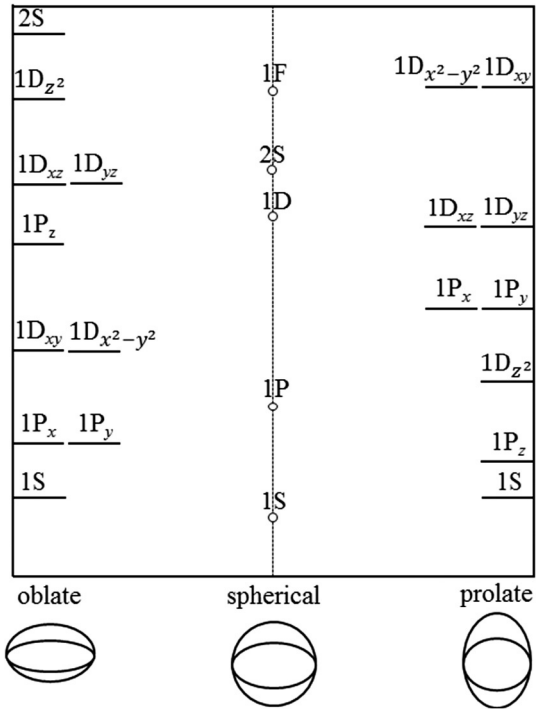

FIG. 11 Schematic energy levels of the shell orbitals with respect to the distortion toward prolate (right) and oblate (left) cluster shapes. *(Taken from P.V. Nhat, N.T. Si, J. Leszczynski, M.T. Nguyen, Another look at structure of gold clusters Au_n from perspective of phenomenological shell model, Chem. Phys. 493 (2017) 140–148.)*

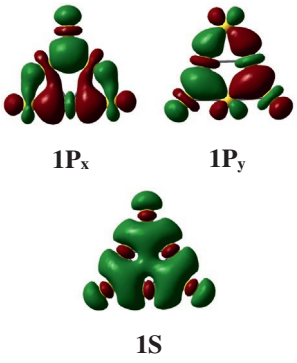

FIG. 12 Shell orbitals of the oblate M_6 clusters. *(Taken from P.V. Nhat, N.T. Si, J. Leszczynski, M.T. Nguyen, Another look at structure of gold clusters Au_n from perspective of phenomenological shell model, Chem. Phys. 493 (2017) 140–148.)*

(LC-BLYP value). A closer look at the electronic structure of these systems allows the differences in going from Cu via Ag to Au to be understood and provides us with an interesting sample for the validity of PSM.

The most stable form of either Cu_8 or Ag_8 is predicted to be a tetrahedron in such a way that it can be treated as a spherical-shaped system. Indeed, Fig. 13 confirms that the electron configuration of this cluster can be described by the initial shell of $1S^2/1P^6$. With eight itinerant electrons and a sphere-like tetrahedron, these species constitute a closed-shell configuration giving them the status of *magic* clusters and thereby particular stability [22].

In contrast to the preference of sphere-like Ag_8 and Cu_8 structures, the most stable D_{2h} form of Au_8 can be regarded as bearing an oblate shape. Therefore, a different landscape emerges as partially occupied quasidegenerate orbitals are involved. From the PSM view for oblate clusters (Fig. 11), Au_8 possesses a $1S^2/1P^4/1D^2$ electron configuration with two electrons distributed on twofold degeneracy $\left\{1D^1_{xy}1D^1_{x^2-y^2}\right\}$ orbitals. Such an electron shell tends to result in a Jahn-Teller distortion, and its frontier orbitals are likely to split into two different energy levels, namely $1D_{xy}$ and $1D_{x^2-y^2}$. As shown in Fig. 13, Au_8 with eight itinerant electrons and an oblate shape is characterized by an electron shell configuration of $1S^2/\{1P^2_x1P^2_y\}/1D^2_{xy}$.

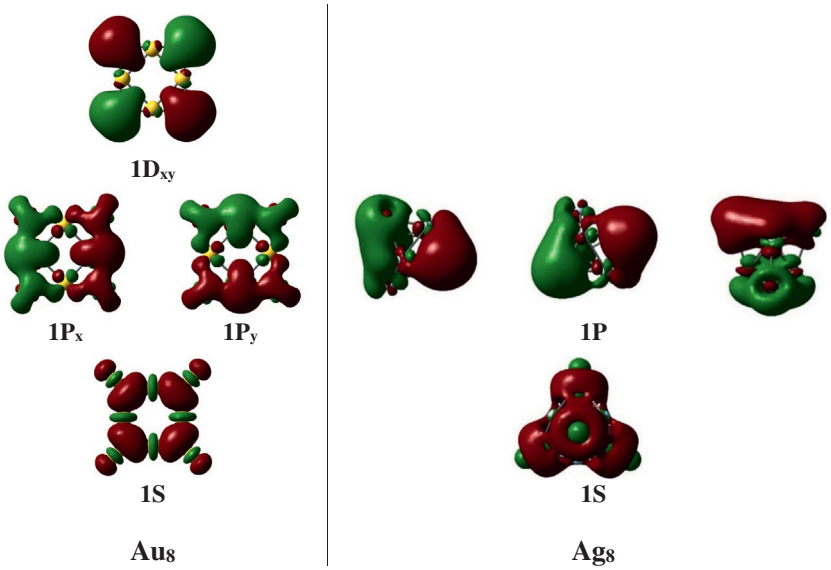

FIG. 13 Shell orbitals of the oblate Au_8 (left) and the spherical-like Ag_8 (right). *(Taken from P.V. Nhat, N.T. Si, M.T. Nguyen, Elucidation of the molecular and electronic structures of some magic silver clusters Ag_n (n= 8, 18, 20), J. Mol. Model. 24 (8) (2018) 1–14.)*

We now examine the electronic structure of M_{20} with M = Cu, Ag, Au species. The ground-state geometry of Ag_{20} and Cu_{20} is almost the same [27], which can be generated by adding three Ag/Cu atoms to a (12,3) Frank-Kasper polyhedron, in such a way that it can also be treated as a spherical shape system. For a nearly spherical cluster with 20 itinerant electrons, it again corresponds to a closed electron shell structure. Fig. 14 shows the shell orbitals for the lowest-energy neutral Ag_{20} cluster denoted as Ag_{20}-**I** in Fig. 6. Both the lowest-energy and highest-energy shells of this neutral cluster are actually *s* orbitals, whereas the three higher-lying orbitals show a *p*-character. Other orbitals lying lower in energy than the HOMO (the 2S shell) clearly have a *d*-character, and they contribute predominantly to the 1D shell orbitals. With 20 itinerant electrons and a closed electron shell, the neutral Ag_{20} thus also prefers a nearly spherical shape over an elliptical form.

The Au_{20} cluster also exhibits an unusually high stability as compared with its neighboring clusters. The most stable form of Au_{20} is a tetrahedron (T_d symmetry) as presented in Fig. 6; it can thus also be treated as a spherical-shape system.

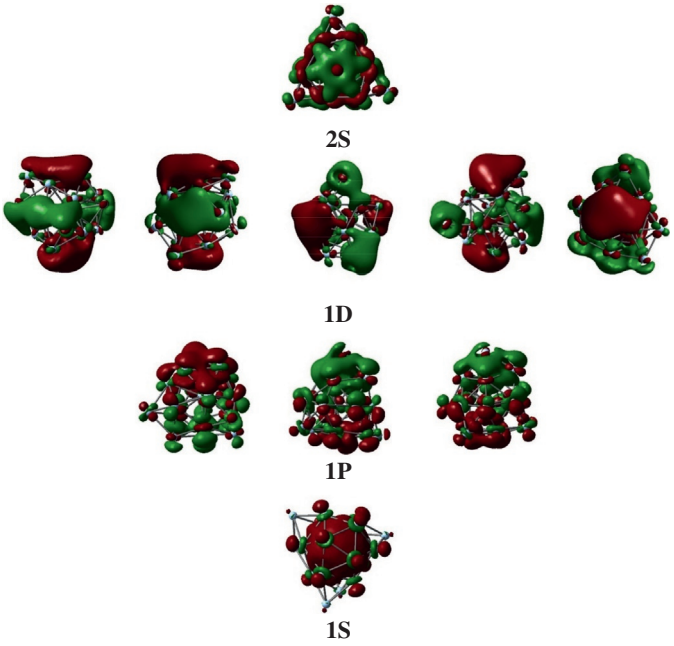

FIG. 14 Electronic structure of the spherical-like cluster Ag_{20} with a closed electron shell configuration $\{1S^2 1P^6 1D^{10} 2S^2\}$. *(Taken from P.V. Nhat, N.T. Si, M.T. Nguyen, Elucidation of the molecular and electronic structures of some magic silver clusters Ag_n (n= 8, 18, 20), J. Mol. Model. 24 (8) (2018) 1–14.)*

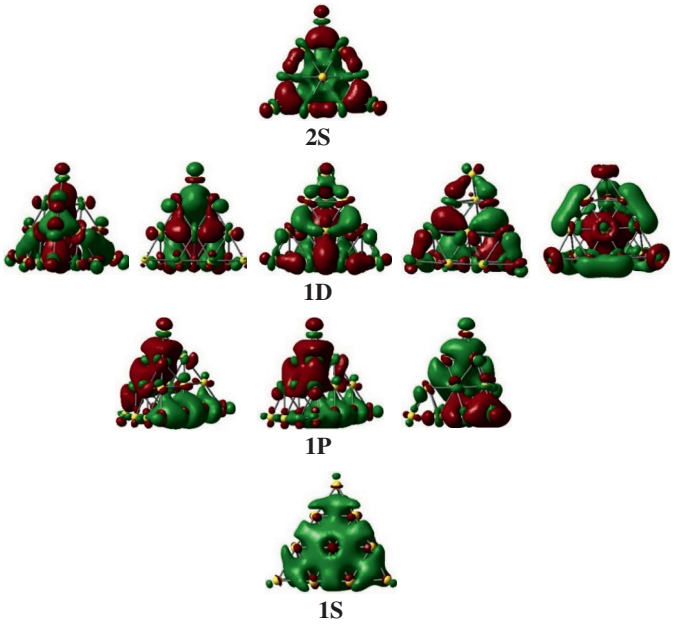

FIG. 15 Electronic structure of the spherical-like cluster Au_{20} with a closed electron shell configuration $\{1S^2 1P^6 1D^{10} 2S^2\}$. *(Taken from P.V. Nhat, N.T. Si, M.T. Nguyen, Elucidation of the molecular and electronic structures of some magic silver clusters Ag_n (n= 8, 18, 20), J. Mol. Model. 24 (8) (2018) 1–14.)*

For a nearly spherical cluster enclosing 20 itinerant electrons, it clearly corresponds to a closed electron shell structure. Indeed, Fig. 15 confirms that the electron configuration of this cluster can be described by the shell $1S^2/1P^6/1D^{10}/2S^2$ configuration. Strictly speaking, notably, five orbitals on the 1D shell split into two different sublevels, namely *e* and t_2, as a result of the T_d-symmetric crystal field. Relativistic effects are strong in heavy atoms such as gold [30,32] and apparently play a vital role in stabilizing the high symmetry tetrahedral T_d structure [84]. On the contrary, for Ag counterpart, due to the significant contributions of its *d* states [85], the effect of geometric packing, i.e., atomic order, is likely competing with an electronic order and leads to a more compact structure for Ag_{20}.

5. Electronic absorption spectra

Electron transitions giving rise to absorption and emission spectra are a direct consequence of orbital configurations. Let us therefore consider in some detail the electronic spectra of these clusters. In addition, optical properties of noble metal clusters also attract a great deal of interest owing to their importance in both basic and applied research studies [4,86]. Study of electronic properties and optical response of these systems is an interesting but also challenging task due to the closely lying *s*, *d*-electrons and strong relativistic effects. One of the most intriguing phenomena is the surface plasmon resonance, i.e., a strong UV absorption due to collective oscillations of conduction electrons [58]. In small clusters, the absorption becomes molecule-like reflecting a well-defined electronic structure [14,87], and the determination of the size at which molecular-type electronic transitions evolve into a plasmon-like absorption is also a fascinating task [88]. In this context, optical properties of noble clusters have been a subject of several studies using both experimental and computational approaches alike [14,58,89].

Small noble metal clusters up to 30 atoms show molecular-like excitations with several typical peaks in their electronic absorption spectra. In addition, substantial differences in optical properties of both Ag_n and Au_n clusters emerge because the *d* states in gold are more directly involved in electronic excitations as compared with those of silver [4]. Such alterations furthermore result from a stronger *s-p-d* hybridization in molecular orbitals of Au_n and maximum relativistic effects of gold. In what follows, we shall examine size by size the predicted absorption spectra of silver and gold species M_n in the range of $n = 1$–20. Theoretical spectra are simulated from time-dependent density functional theory (TD-DFT) calculations using the long-range corrected XC functional LC-BLYP and the cc-pVDZ-PP basis set. A number of results have previously been reported and are confirmed by the present study.

The experimental spectrum of the gold atom contains two well-defined peaks at 4.8 and 5.4 eV, corresponding to the spin-orbit split $^2S_{1/2} \rightarrow {}^2P_{1/2}$ and $^2S_{1/2} \rightarrow {}^2P_{3/2}$ transitions [90]. The simulated spectrum of Au atom shown in Fig. 16,

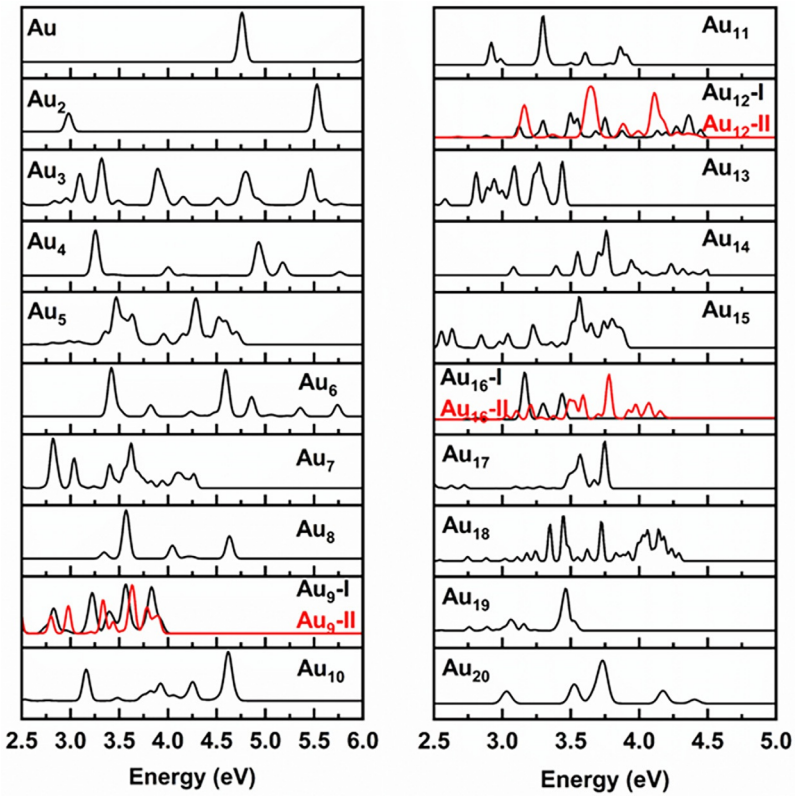

FIG. 16 TD-DFT absorption spectra for the lowest-lying structures of gold Au_n clusters.

however, exhibits only one intense transition near 5.3 eV, which can be attributed to the S → P transition. This is presumably due to the fact that TD-DFT calculations do not accurately account for the spin-orbit coupling effects.

The absorption spectrum of the gold dimer has also been experimentally studied, and several absorption bands are found to be situated in the energy region of 2.5–5.5 [86,91,92]. With a reasonable certainty, we would assign the so-called $X \rightarrow B$ transition measured at 3.18 eV to the predicted value near 3.0 eV, whereas the $X \rightarrow D$ measured transition at 5.3 eV corresponds to the computed one at 5.2 eV. However, both $X \rightarrow A$ and $X \rightarrow C$ transitions observed experimentally at 2.44 and 4.80 eV are not reproduced in the TD-DFT absorption spectrum of Au_2.

The LC-BLYP absorption spectrum for Au_3 consists of several significant peaks in the range between 3.0 and 4.5 eV, for which experimental data have also been available [86]. Accordingly, the low-intensity peak at 3.1 eV is likely associated with the 3.05–3.50 eV transitions found in previous experiments [86,92]. In addition, the higher-intensity absorption line at 3.6 eV can be accounted for by the measured transition at 3.64 eV [86,92].

The absorption spectrum of gold tetramer exhibits a highly intense peak near 3.2 eV and another weaker transition at 4.1 eV. The experimental spectrum [86] also exhibits a prominent transition at 3.3 eV, whereas the peak at 4.05 eV splits into two components at 4.0 and 4.1 eV. For Au_5, the predicted transitions with particularly large oscillator strengths are located at 2.7, 3.3, and 3.5 eV. Previous measurement [86] also detected such transitions at a somewhat lower-energy region between 2.95 and 3.25 eV. In addition, one can detect some low-intensity peaks above 4.0 eV.

To date, the experimental UV spectrum for Au_6 is not available, even though previous analyses indicate this is a "magic" cluster with a rather large excitation energy [93]. Thus, it can serve as a proper model system for assessing the reliability of excited states calculations for gold clusters. The lowest excited state of Au_6 is located at ~3.4 eV (LC-BLYP). A comparable gap is obtained with the ωB97X functional (3.3 eV) and EOM-CCSD (3.3 eV) approaches, whereas both TPSS and B3LYP functionals yield significantly reduced transition energies to 2.4 and 2.8 eV, respectively [89].

The measured and computed absorption spectra of Au_7 have been reported in the literature [58,86]. Accordingly, locations of strong peaks are observed in the range of 2.6–3.6 eV that are also well reproduced in the simulated spectrum (Fig. 16).

As compared with the odd numbered clusters such as Au_3, Au_5, and Au_7, the absorption of the gold octamer is much simpler. The calculated spectrum for the ground-state Au_8-**I** covers a range below 4.1 eV with three characteristic peaks centered at 3.4, 3.6, and 4.1 eV that were also experimentally seen with close values [86]. For Au_9, the experimental spectrum shows a large amount of peaks situated at 2.9, 3.2, 3.7, 3.9, and 5.1 eV [86]. Previously, the observed

photo-dissociation spectrum emphasized two broad absorption bands at ~2.2 and 3.0 eV [94]. The spectra of two lowest-energy structures Au_9-**I** and Au_9-**II** (Fig. 4) simulated at the LC-BLYP/cc-pVDZ-PP level and shown in Fig. 12 suggest that the observed spectrum likely arises from a superposition of both isomers rather than from a sole carrier. Accordingly, the peaks located at 2.2, 2.7 and 3.2 eV can be assigned for intense transitions at 2.2, 2.8, and 3.2 eV in the predicted spectrum of Au_9-**I**. On the contrary, the observed bands at 2.9 eV, which are absent in the spectrum of Au_9-**I**, are consistent with the transition at 3.0 eV coming from the second isomer Au_9-**II**.

In the case of Au_{10}, TD-DFT calculations give a main peak at 3.2 eV and followed by a gap of ~0.6 eV to a characteristic trio of lower-intensity features separated by about 0.05–0.1 eV. For Au_{11}, previous experimental study observed a local absorption maximum at ~2.9 eV [12]. This peak is quite well reproduced in the calculated spectrum of Au_{11}-**I** as it is located around 2.8 eV. In addition, a weaker signal at ~3.0 eV and a stronger one at 3.3 eV could also be detected. Calculations performed for both Au_{12}-**I** (3D) and Au_{12}-**II** (2D) isomers (Fig. 16) show that the spectrum of Au_{12}-**I** contains a strong doublet between 3.5 and 3.6 eV, along with lower-intensity peaks at 3.1 and 3.3 eV. The 2D isomer Au_{12}-**II** exhibits a simpler spectrum with two prominent bands centered at ~3.2 and 3.7 eV.

Calculated absorption spectra for larger Au_n clusters including $n = 13$–20 in the energy range of 2.5–5.0 eV are also presented in Fig. 16. In general, the absorption lines of odd-numbered systems, when compared with those of the even-numbered counterparts, are typically more complicated and appear in the lower-energy region. For example, the optical absorption spectra of odd clusters with $n = 13$, 15, 17, and 19 show particularly high peaks between 2.4 and 2.7 eV that are significantly shifted to ~3.7 eV for Au_{14} and Au_{16}. Concerning Au_{18} and Au_{20}, while the former gives several lines with a maximum at 3.7 eV and two lower-intensity transitions below 3.6 eV, the latter exhibits a strong absorption located at ~3.7 eV. Our present LC-BLYP calculations are thus comparable to those obtained with the CAM-B3LYP and LC-M06L functionals. Previously, the plasmon-like band of the tetrahedron Au_{20} was located at 3.5 and 3.8 eV by the CAM-B3LYP and LC-M06L, respectively [89,95]. However, LDA and GGA predictions produced peaks at much lower energies [96]. For example, while the BP86 calculation identified the most intense transition in Au_{20} at 2.9 eV [97], LDA predicted such a band at 2.8 eV [58].

Several studies on both experimental and theoretical aspects have been devoted to the optical properties of neutral silver clusters [14,90,95]. Generally, these nanostructures display the stepwise, multiple-band spectra that bear a common feature of noble metal clusters [90,98,99] as shown in Fig. 17.

The simulated spectrum of the Ag atom produces one main peak at 3.8 eV (331 nm). This band can be assigned to the measured band at 326 nm (3.80 eV) or 328 nm (3.78 eV) in Ar and Kr matrices, respectively [100]. For the dimer Ag_2, the lowest excited state is observed at 3.0 eV, which is marginally closer to the given experimental value of 2.96 eV [90] than the previous PBE prediction of 3.1 eV [101]. In addition, we detect two other intense transitions in the higher-energy region at 4.3 and 4.8 eV. The theoretical UV-visible optical absorption of the trimer Ag_3 becomes more complicated with two intense signals at 3.6 and 3.8 eV. Besides, some lower-intensity peaks can be detected below 3.0 eV. To date, no experimental spectrum of the trimer is available.

Let us now examine the UV-vis spectra of Ag_n in the sizes $n = 4$–14 in comparison with existing experimental results previously obtained by Harb et al. [14]. The simulated absorption spectra the D_{2h} isomer Ag_4-**I** exhibit the highest transition at 3.1 eV, which has also been observed by all TD-DFT calculations [14]. Other lesser intense signals at 4.0, 4.2, 4.8, and 5.0 eV are further detectable. As compared with the experiment, the main transition is well reproduced at 3.1 eV, while other lower-intensity peaks are measured at 4.2, 4.5, and 4.8 eV. In the case of Ag_5, two extensive bands were experimentally measured at 3.3 and 3.8 eV. TD-DFT calculations for Ag_5-**I** also reproduce two main transitions at 3.2 and 3.8 eV. Accordingly, the agreement between theory and experiment is quite good for both Ag_4 and Ag_5 systems.

The computed spectrum of the D_{3h} Ag_6-**I** contains a distinct transition at 3.6 eV along with some smaller signals at 3.1 and 5.1 eV. Such a prediction is not properly consistent with the experimental one, which shows two distinct peaks at 3.6 and 4.2 eV, as well as smaller bands at 4.9 and 5.1 eV. Harb et al. [14] also pointed out in taking the presence of the less stable C_{5v} isomer into account, the agreement between theoretical and experimental spectra becomes better. Regarding Ag_7, the experimental spectrum contains primarily one broad band with a doublet at 3.6 and 3.8 eV. As discussed above, two quasidegenerate isomers D_{5h} Ag_7-**I** and C_{3v} Ag_7-**II** (Fig. 4) with a tiny energy gap of 0.07 eV are strongly competing for the ground state of Ag_7. However, the calculated spectrum of Ag_7-**I** does not match the experiment well. Instead, that of Ag_7-**II** reproduces better the experimental spectrum and the agreement between both computed and measured spectra turns out to be more convincing. The doublet between 3.6 and 3.8 eV is properly generated and can be assigned to the broad signal at 3.7 eV in the C_{3v} spectrum. The reason for such a presence of only one isomer of a degenerate couple in the molecular beam is not clear to us.

For Ag_8, LC-LYP/cc-pVDZ-PP calculations predict that important absorption bands of Ag_8-**I** occur at 4.1 and 3.1 eV that are comparable to previous predictions at 4.0 and 3.0 eV (BP86/LANL2DZ), 4.0 and 3.1 eV (B3LYP/LANL2DZ), 4.2 and 3.3 eV (EOM-CCSD), 4.0 and 3.1 eV (CASPT2) [102]. Such transitions can also be assigned for intense experimental

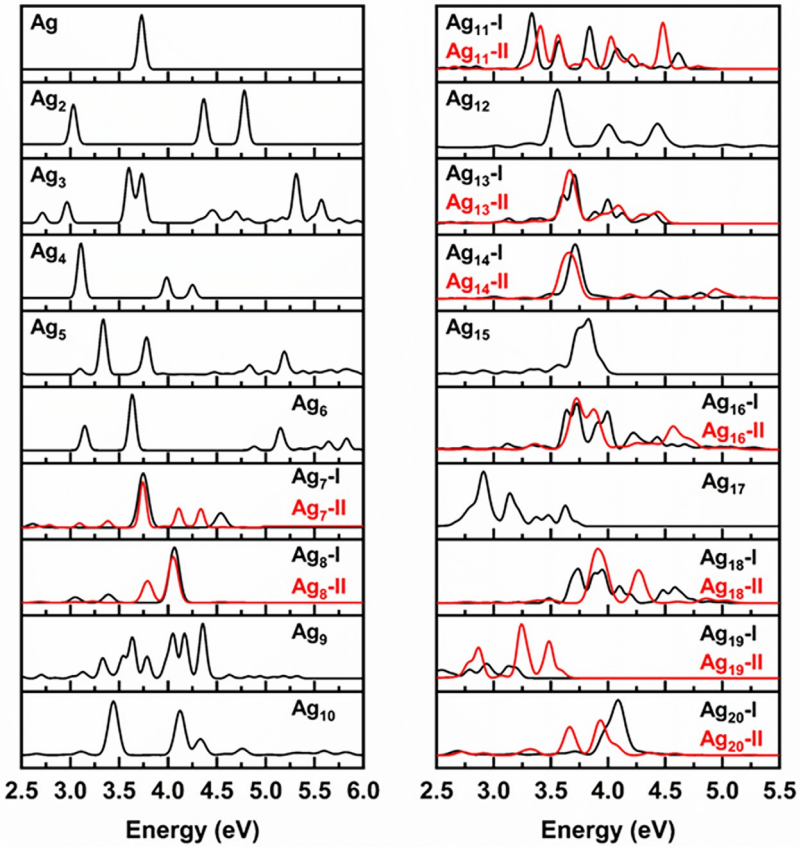

FIG. 17 TD-DFT absorption spectra for the lowest-lying structures of silver Ag_n clusters.

peaks observed at 4.0 and 3.0 eV, respectively [14]. However, the spectrum of this form does not contain a narrow peak at 3.6 eV detected in the experimental spectrum. Instead, such transition can be derived from the D_{2d} Ag_8-**II** whose absorption spectrum exhibits noticeable peaks centered at 3.1, 3.8, and 4.1 eV. Thus, both the lowest-energy isomers are likely present under experimental conditions, and the observed spectrum arises from a superposition of both spectra, rather than from a sole carrier.

The experimental spectrum of Ag_9 contains a low intensity peak at 2.8 eV and several narrow ones between 3.3 and 4.3 eV. We actually reproduce this absorption spectrum in considering the lowest-energy Ag_9-**I** located in this study. The latter can account for the measured bands in the region of 3.3–4.3 eV, but not for the experimental band at 2.8 eV. The experimental spectrum of Ag_{10} shows three distinct lines at 3.8, 4.0, and 4.2 eV, which are very similar to that of Ag_9. Since all three peaks are present in the Ag_9 spectrum at the same positions, a plausible explanation is that in reality the Ag_9 size was observed. As shown in Fig. 17, the calculated spectrum of Ag_{10}-**I** featuring three important peaks centered at 3.5, 4.1, and 4.2 eV does not reproduce well the reported spectrum in ref. [14], which does not show any transition below 3.5 eV.

The absorption spectra of two lowest-lying isomers Ag_{11}-**I** and Ag_{11}-**II**, which are basically degenerate, are presented in Fig. 12. Overall, the former reproduces the experimental data better than the latter. Accordingly, sharp lines at 3.6 and 4.2 eV in the computed spectrum of Ag_{11}-**I** can be assigned to those at 3.7 and 4.3 eV in the measured one [103,104]. The Ag_{11} cluster was also studied in detail by Idrobo et al. [105], and although the experimental spectrum could be due to a superposition from different isomers, the lowest-energy one brings in the most significant contribution. For Ag_{12}, the predicted spectrum of the lowest-energy Ag_{12}-**I** contains one intense peak near 3.5 eV and two lower ones at 4.0 and 4.4 eV, which are in good agreement with the experiment [14]. Accordingly, the spectrum obtained for Ag_{12} in Ar exhibits a very similar shape with three distinct peaks in the region of 3.4–4.4 eV.

In the case of Ag_{13}, LC-BLYP calculations for both lowest-energy structures find an intense transition at ~3.6 eV and some lower ones between 4.0 and 4.5 eV. Overall, the agreement with the experiment is convincing as the measurement obtained for Ag_{13} consists of a well-defined peak at 3.4 eV and some lower-intensity lines between 3.9 and 4.4 eV. Positions of the distinct transitions are rather well reproduced if we take a small blue shift into account. For silver cluster containing

14 atoms, it was experimentally found to have a very similar absorption spectrum to those of Ag_{12} and Ag_{13} with a broad band near 3.5 eV, along with two shoulders at 4.0 and 5.0 eV [14]. The spectra computed for both lowest-energy Ag_{14}-**I** and Ag_{14}-**II** exhibit very comparable shapes with a main transition near 3.6 eV and some less intense bands at higher energy.

Next we consider the absorption spectra for the larger series of Ag_n ($n = 15$–20) systems in which our LC-BLYP results can be compared with experimental data previously reported by Fedrigo and coworkers [106]. Overall, the measured spectra of these clusters are characterized by the dominance of a broad band lying between 3.2 and 3.8 eV, accompanied by some shoulders at higher energies with much lower intensities. This common feature is coupled to a slight shift to the higher energy region of the highest transition when the cluster size increases. While our predicted spectra for even systems are quite consistent with the experiment, the agreement of those of odd counterparts is less convincing. Let us look at Ag_{15} as for an example. While present calculations give a main transition centered at 3.8 eV for Ag_{15}-**I** (Fig. 17), the experimental spectrum shows a broad band at ~3.5 eV. Similarly, the predicted transitions between 2.5 and 3.3 eV in the absorption spectra of Ag_{17} and Ag_{19} are also not observed experimentally. However, the mostly intense peaks between 3.5 and 3.7 eV in the measured spectra of these clusters are well detected in the TD-DFT spectra.

As reported in ref. [106], the experimental absorption spectrum of Ag_{18} is characterized by a dominant peak at 3.6 eV and accompanied by a shoulder at ~4.1 eV. Our LC-BLYP calculations for the lowest-energy isomer Ag_{18}-**I** give a main peak at 3.7 eV along with a rather lower-intensity peak at 4.1 eV, which are in very good agreement with experiment. However, the predicted transition at 3.9 eV is, nevertheless, not observed experimentally. Previous CAM-B3LYP calculations similarly detected several peaks scattered on the 3.5–4.5 eV range with two maxima at 3.6 and 4.1 eV [107]. We also regenerate the absorption spectrum of the lower-lying isomer Ag_{18}-**II** and find that it differs much from that of Ag_{18}-**I** and does not match the experiment.

The experimental absorption spectrum of Ag_{20} was also recorded and reported in ref. [106]. Accordingly, the recorded spectrum is composed of a broad band near 3.7 eV and a much less intense one ~4.0 eV. Our LC-BLYP computations for the Ag_{20}-**I** yield a strong transition centered at 4.1 eV, which is not in line with the experiment. The computed spectrum for the tetrahedron Ag_{20}-**II** with some dominant peaks at 3.7 and 4.0 eV, for its part, agrees better with the experiment. Overall, following an increase of cluster size, the absorption spectrum becomes simpler with only one main strong band, in correlation with the fact that the silver structure becomes more compact and spherical. Overall, the magic clusters represent somewhat different absorption behaviors. The UV-Vis spectra of Ag_8, Ag_{20}, and Au_{20} systems are in fact much simpler, and each is characterized by the dominance of a broad, highly intense transition.

There is no direct correlation between the electron shell model and absorption spectra. It seems that the model is too simple to account for the complex electronic excitations of clusters.

6. Concluding remarks

We report in this chapter a comprehensive review on the structural evolution, stability trend, and electronic properties of a series of small silver and gold clusters in the range size from 2 to 20 atoms. The lowest-energy structures and some basic thermodynamic parameters are either confirmed or determined using the LC-BLYP and PBE functionals in conjunction with the pseudo-potential cc-pVDZ-PP basis set. The structural evolution of both series is analyzed in terms of the electron shell model. Their optical spectra are also simulated and compared with available experimental data. A number of interesting results emerge as follows:

(i) While the silver Ag_n early adopts three-dimensional (3D) structures at $n = 6$, a structural transition from 2D to 3D in gold systems appears to take place at around Au_{10}. From $n = 7$, both Ag_n and Au_n species exhibit very different geometries in their ground state and follow distinct growth patterns. The Ag_n with $n = 7$–16 prefers 3D structures that can be constructed by adding extra Ag atoms either on the D_{5h} bipyramid Ag_7-**I** or the T_d isomer Ag_8-**I**. As the cluster size increases, a common trend of forming close-packed structures emerges from a 13-atom icosahedral core by adding extra atoms on triangular faces. As compared with the silver Ag_n, the gold Au_n generally exhibits more symmetric ground state structures. A local minimum of a specific Au_n system is usually generated from the lowest-lying isomer of the smaller size Au_{n-1} by adding an extra gold atom at different spatial position. In particular, the global energy minima obtained for species with $n = 18$–20 are formed by capping extra gold atoms on the 16-vertex Frank-Kasper Au_{16} core.

(ii) Some basic energetic properties including binding energies per atom, the one-step fragmentation energy, and stepwise dissociation energies are also presented. Compared with experimental data, the PBE functional turns out to be more reliable in predicting the binding energies per atom and dissociation energies, whereas the LC-BLYP functional is

likely to be more suitable for structural predictions. Analysis of basic energetics demonstrates that the sizes Au_6, Ag_8, Ag_{20}, and Au_{20} attain remarkable thermodynamic stability with more symmetric structures than their neighbors.

(iii)

The stability pattern and electronic structure of these magic clusters are also rationalized and enlightened in terms of the phenomenological shell model (PSM). Accordingly, the Ag_8 with eight itinerant electrons features a sphere-like form ground state (T_d symmetry) and a closed $1S^2/1P^6$ electronic configuration. Similarly, the nearly spherical Au_{20}, which favors a tetrahedron shape (T_d symmetry), also has a closed $1S^2/1P^6/1D^{10}/2S^2$ electron shell. Consequently, such species exhibit high symmetry structures and are particularly stable members of the series examined.

(iv)

The computed electronic spectra of the clusters present several interesting observations. Both systems exhibit a strong optical response in the UV-visible range, but some major inherent differences appear in their spectra. While the spectra of gold clusters are normally characterized by sharply well separated peaks, those of silver clusters are dominated by a relatively broad peak, accompanied with some lower intensity absorption bands. The main absorption peaks in each series seem to appear in a similar energy region, with some small shifts. However, the spectral pattern becomes much simpler with the emergence of a dominant peak when the clusters size becomes larger and more spherical. Such differences in behavior of the two series of clusters allow a suitable choice for the cluster to be used, for example, as sensors for detecting some organic compounds and pollutants.

Funding information

This work was funded by VinGroup (Vietnam) and supported by VinGroup Innovation Foundation (VinIF) under project code VINIF.2020.DA21.

References

[1] X. Yang, W. Cai, X. Shao, Structural variation of silver clusters from Ag_{13} to Ag_{160}, J. Phys. Chem. A 111 (2007) 5048.
[2] V.E. Matulis, A.S. Mazheika, O.A. Ivashkevich, DFT study of electronic structure and geometry of anionic silver clusters Ag_n^- (n = 11, 12, 17), J. Mol. Struct. 850 (2008) 61.
[3] S. Zhao, Y.L. Ren, Y. Ren, J.J. Wang, W.P. Yin, Density functional study of hydrogen binding on gold and silver – gold clusters, J. Phys. Chem. A 114 (2010) 4917–4923.
[4] M.S. Liao, P. Bonifassi, J. Leszczynski, P.C. Ray, M.J. Huang, D.J. Watts, Structure, bonding, and linear optical properties of a series of silver and gold nanorod clusters: DFT/TDDFT studies, J. Phys. Chem. A 114 (48) (2010) 12701–12708.
[5] B.M. Barngrover, C.M. Aikens, Incremental binding energies of gold (I) and silver (I) thiolate clusters, J. Phys. Chem. A 115 (42) (2011) 11818–11823.
[6] S.K.R. Namasivayam, S. Ganesh, B. Avimanyu, Evaluation of anti-bacterial activity of silver nanoparticles synthesized from *Candida glabrata* and *Fusarium oxysporum*, Int. J. Med. Res. 1 (3) (2011) 131–136.
[7] M.A. Ansari, H.M. Khan, A.A. Khan, A. Malik, A. Sultan, M.M. Shahid, Evaluation of antibacterial activity of silver nanoparticles against MSSA and MSRA on isolates from skin infections, Biol. Med. 3 (2011) 141–146.
[8] J. Hainfeld, D. Slatkin, T. Focella, H. Smilowitz, Gold nanoparticles: a new X-ray contrast agent, Br. J. Radiol. 79 (939) (2006) 248.
[9] J. Zheng, R.M. Dickson, Individual water-soluble dendrimer-encapsulated silver nanodot fluorescence, J. Am. Chem. Soc. 124 (47) (2002) 13982.
[10] T. Vosch, Y. Antoku, J.C. Hsiang, C.I. Richards, J.I. Gonzalez, R.M. Dickson, Strongly emissive individual DNA-encapsulated Ag nanoclusters as single-molecule fluorophores, Proc. Natl. Acad. Sci. 104 (31) (2007) 12616–12621.
[11] O. Fenwick, E. Coutiño-Gonzalez, D. Grandjean, W. Baekelant, F. Richard, S. Bonacchi, D.D. Vos, P. Lievens, M. Roeffaers, J. Hofkens, P. Samorif, Tuning the energetics and tailoring the optical properties of silver clusters confined in zeolites, Nat. Mater. 15 (22) (2016) 1017–1022.
[12] B.A. Collings, K. Athanassenas, D.M. Rayner, P.A. Hackett, Optical spectroscopy of Ag_7, Ag_9^+, and Ag_9. A test of the photodepletion method, Chem. Phys. Lett. 227 (4–5) (1994) 490–495.
[13] S. Krückeberg, G. Dietrich, K. Lützenkirchen, L. Schweikhard, C. Walther, J. Ziegler, The dissociation channels of silver clusters Ag_n^+, $3 \leq n \leq 20$, Int. J. Mass Spectrom. 155 (3) (1996) 141–148.
[14] M. Harb, F. Rabilloud, D. Simon, A. Rydlo, S. Lecoultre, F. Conus, V. Rodrigues, C. Félix, Optical absorption of small silver clusters: Ag_n, (n = 4–22), J. Chem. Phys. 129 (19) (2008), 194108.
[15] A. Shayeghi, D.A. Götz, R.L. Johnston, R. Schäfer, Optical absorption spectra and structures of Ag_6^+ and Ag_8^+, Eur. Phys. J. D 69 (6) (2015) 1–5.
[16] R. Fournier, Theoretical study of the structure of silver clusters, J. Chem. Phys. 115 (5) (2001) 2165–2177.
[17] V. Bonačić-Koutecky, V. Veyret, R. Mitrić, Ab initio study of the absorption spectra of (n=5–8) clusters, J. Chem. Phys. 115 (22) (2001) 10450–10460.

[18] M. Chen, J.E. Dyer, K. Li, D.A. Dixon, Prediction of structures and atomization energies of small silver clusters,(Ag) n, n< 100, J. Phys. Chem. A 117 (34) (2013) 8298–8313.
[19] Y. Jin, Y. Tian, X. Kuang, C. Zhang, C. Lu, Ab initio search for global minimum structures of pure and boron doped silver clusters, J. Phys. Chem. A 119 (25) (2015) 6738–6745.
[20] K. Duanmu, D.G. Truhlar, Validation of methods for computational catalyst design: geometries, structures, and energies of neutral and charged silver clusters, J. Phys. Chem. C 119 (17) (2015) 9617–9626.
[21] A. Fielicke, I. Rabin, G. Meijer, Far-infrared spectroscopy of small neutral silver clusters, J. Phys. Chem. A 110 (26) (2006) 8060–8063.
[22] M.L. McKee, A. Samokhvalov, Density functional study of neutral and charged silver clusters Ag_n with n = 2–22. Evolution of properties and structure, J. Phys. Chem. A 121 (26) (2017) 5018–5028.
[23] J. van der Tol, D. Jia, Y. Li, V. Chernyy, J.M. Bakker, M.T. Nguyen, P. Lievens, E. Janssens, Structural assignment of small cationic silver clusters by far-infrared spectroscopy and DFT calculations, Phys. Chem. Chem. Phys. 19 (29) (2017) 19360–19368.
[24] X.-B. Li, H.-Y. Wang, X.-D. Yang, Z.-H. Zhu, Y.-J. Tang, Size dependence of the structures and energetic and electronic properties of gold clusters, J. Chem. Phys. 126 (8) (2007), 084505.
[25] P. Gruene, D.M. Rayner, B. Redlich, A.F. van der Meer, J.T. Lyon, G. Meijer, A. Fielicke, Structures of neutral Au_7, Au_{19}, and Au_{20} clusters in the gas phase, Science 321 (5889) (2008) 674–676.
[26] P.V. Nhat, N.T. Si, J. Leszczynski, M.T. Nguyen, Another look at structure of gold clusters Au_n from perspective of phenomenological shell model, Chem. Phys. 493 (2017) 140–148.
[27] P.V. Nhat, N.T. Si, M.T. Nguyen, Elucidation of the molecular and electronic structures of some magic silver clusters Ag_n (n= 8, 18, 20), J. Mol. Model. 24 (8) (2018) 1–14.
[28] T. Tsuneda, Theoretical investigations on geometrical and electronic structures of silver clusters, J. Comput. Chem. 40 (1) (2019) 206–211.
[29] A. Mitra, G. Jana, R. Pal, P. Gaikwad, S. Sural, P.K. Chattaraj, Determination of stable structure of a cluster using convolutional neural network and particle swarm optimization, Theor. Chem. Acc. 140 (3) (2021) 1–12.
[30] P. Pyykkö, Relativistic effects in structural chemistry, Chem. Rev. 88 (3) (1988) 563–594.
[31] M.P. Johansson, I. Warnke, A. Le, F. Furche, At what size do neutral gold clusters turn three-dimensional? J. Phys. Chem. C 118 (50) (2014) 29370–29377.
[32] P. Schwerdtfeger, M. Dolg, W.H.E. Schwarz, G.A. Bowmaker, P.D.W. Boyd, Relativistic effects in gold chemistry. I. Diatomic gold compounds, J. Chem. Phys. 91 (3) (1989) 1762–1774.
[33] H. Häkkinen, M. Moseler, U. Landman, Bonding in Cu, Ag, and Au clusters: relativistic effects, trends, and surprises, Phys. Rev. Lett. 89 (3) (2002), 033401.
[34] I. Katakuse, T. Ichihara, Y. Fujita, T. Matsuo, T. Sakurai, H. Matsuda, Mass distributions of copper, silver and gold clusters and electronic shell structure, Int. J. Mass Spectrom. 67 (3) (1985) 229–236.
[35] I. Katakuse, T. Ichihara, Y. Fujita, T. Matsuo, T. Sakurai, H. Matsuda, Mass distributions of negative cluster ions of copper, silver, and gold, Int. J. Mass Spectrom. 74 (1) (1986) 33–41.
[36] J.A. Alonso, Electronic and atomic structure, and magnetism of transition-metal clusters, Chem. Rev. 100 (2) (2000) 637–678.
[37] W.A. de Heer, W.D. Knight, M.Y. Chou, M.L. Cohen, Electronic shell structure and metal clusters, Solid State Phys. 40 (1987) 93–181.
[38] J.A. Alonso, N.H. March, Electrons in Metals and Alloys, Academic, London, 1989.
[39] W. Bouwen, F. Vanhoutte, F. Despa, S. Bouckaert, S. Neukermans, L.T. Kuhn, H. Weidele, P. Lievens, R.E. Silverans, Stability effects of $Au_nX_m^+$ (X= Cu, Al, Y, In) clusters, Chem. Phys. Lett. 314 (3–4) (1999) 227–233.
[40] M.D. Morse, Clusters of transition-metal atoms, Chem. Rev. 86 (6) (1986) 1049–1109.
[41] B. Simard, P.A. Hackett, A.M. James, P.R. Langridge-Smith, The bond length of silver dimer, Chem. Phys. Lett. 186 (4–5) (1991) 415–422.
[42] V. Srdanov, D. Pešić, Analysis of the EX and CX band system isotopically enriched of Ag_2, J. Mol. Spectrosc. 90 (1) (1981) 27–32.
[43] K.P. Huber, G. Herzberg, Constants of diatomic molecules, in: Molecular Spectra and Molecular Structure, Springer, New York, NY, 1979, pp. 8–689.
[44] H. Iikura, T. Tsuneda, T. Yanai, K. Hirao, A long-range correction scheme for generalized-gradient-approximation exchange functionals, J. Chem. Phys. 115 (8) (2001) 3540–3544.
[45] K.A. Peterson, C. Puzzarini, Systematically convergent basis sets for transition metals. II. Pseudopotential-based correlation consistent basis sets for the group 11 (Cu, Ag, Au) and 12 (Zn, Cd, Hg) elements, Theor. Chem. Acc. 114 (4) (2005) 283–296.
[46] P.V. Nhat, N.T. Si, M.T. Nguyen, Structural evolution and stability trend of small-sized gold clusters Au_n (n= 20-30), J. Phys. Chem. A 124 (2020) 1289–1299.
[47] R.M. Olson, M.S. Gordon, Isomers of Au_8, J. Chem. Phys. 126 (21) (2007), 214310.
[48] G. Zanti, D. Peeters, Electronic structure analysis of small gold clusters Au_m (m ≤ 16) by density functional theory, Theor. Chem. Acc. 132 (2013) 13001–13015.
[49] B. Assadollahzadeh, P. Schwerdtfeger, A systematic search for minimum structures of small gold clusters Au_n (n = 2–20) and their electronic properties, J. Chem. Phys. 131 (6) (2009), 064306.
[50] D. Tian, H. Zhang, J. Zhao, Structure and structural evolution of Ag_n (n = 3–22) clusters using a genetic algorithm and density functional theory method, Solid State Commun. 144 (3–4) (2007) 174–179.
[51] V. Bonacic-Koutecky, Effective core potential-configuration interaction study of electronic structure and geometry of small neutral and cationic Agn clusters: predictions and interpretation of measured properties, J. Chem. Phys. 98 (10) (1993) 7981–7984.

[52] E.M. Fernández, J.M. Soler, I.L. Garzón, Trends in the structure and bonding of noble metal clusters, Phys. Rev. B 70 (16) (2004), 165403.
[53] Z. Torbatian, S.J. Hashemifar, H. Akbarzadeh, First-principles insights into interaction of CO, NO, and HCN with Ag_8, J. Chem. Phys. 140 (8) (2014), 084314.
[54] H.M. Lee, M. Ge, B. Sahu, P. Tarakeshwar, K.S. Kim, Geometrical and electronic structures of gold, silver, and gold − silver binary clusters: origins of ductility of gold and gold − silver alloy formation, J. Phys. Chem. B 107 (37) (2003) 9994–10005.
[55] M. Yang, K. Jackson, J. Jellinek, First-principles study of intermediate size silver clusters: shape evolution and its impact on cluster properties, J. Chem. Phys. 125 (14) (2006), 144308.
[56] H. Zhang, D. Tian, Structural evolution of Ag_n^v (v = ±1, 0; n = 3–14) clusters using genetic algorithm and density functional theory method, Comput. Mater. Sci. 42 (3) (2008) 462–469.
[57] A. Deka, R.C. Deka, Structural and electronic properties of stable Au_n (n = 2–13) clusters: a density functional study, J. Mol. Struct. THEOCHEM 870 (1–3) (2008) 83–93.
[58] J.C. Idrobo, W. Walkosz, S.F. Yip, S. Öğüt, J. Wang, J. Jellinek, Static polarizabilities and optical absorption spectra of gold clusters (Au_n, n = 2–14 and 20) from first principles, Phys. Rev. B 76 (20) (2007), 205422.
[59] L. Xiao, B. Tollberg, X. Hu, L. Wang, Structural study of gold clusters, J. Chem. Phys. 124 (11) (2006), 114309.
[60] P.L. Rodríguez-Kessler, A.R. Rodríguez-Domínguez, D.M. Carey, A. Muñoz-Castro, Structural characterization, reactivity, and vibrational properties of silver clusters: a new global minimum for Ag_{16}, Phys. Chem. Chem. Phys. 22 (46) (2020) 27255–27262.
[61] P.V. Nhat, N.T. Si, L.V. Duong, M.T. Nguyen, Comment on "Structural characterization, reactivity and vibrational properties of silver clusters: a new global minimum for Ag16" by P. L. Rodríguez-Kessler, A. R. Rodríguez-Domínguez, D, MacLeod Carey and A. Muñoz-Castro, Phys. Chem. Chem. Phys., 2020, 22, 27255, DOI: D0CP04018E, Phys. Chem. Chem. Phys. 23 (2021) 12900–12903.
[62] H.-Y. Zhao, H. Ning, J. Wang, X.-J. Su, X.-G. Guo, Y. Liu, Structural evolution of Au_n (n = 20–32) clusters: lowest-lying structures and relativistic effects, Phys. Lett. A 374 (8) (2010) 1033–1038.
[63] K. Baiasvbramanicin, Relativistic Effects in Chemistry, Part B, Wiley, New York, 1997.
[64] J. Wang, G. Wang, J. Zhao, Density-functional study of Au_n (n = 2–20) clusters: lowest-energy structures and electronic properties, Phys. Rev. B 66 (3) (2002), 035418.
[65] J.W. Arblaster, Thermodynamic properties of gold, J. Phase Equilib. Diffus. 37 (2) (2016) 229–245.
[66] F. Baletto, R. Ferrando, Structural properties of nanoclusters: energetic, thermodynamic, and kinetic effects, Rev. Mod. Phys. 77 (1) (2005) 371.
[67] R. Belosludov, T. Yoshinari, T. Hiwada, Y. Kawazoe, K. Ohno, S.I. Nagasaka, Cluster investigations in cyclodextrin inclusion compounds: theory and experiment, in: Clusters and Nanomaterials, 2002, pp. 109–131.
[68] C. Kittel, Introduction to Solid State Physics, John Wiley & Sons, New York, 1976.
[69] P. Schwerdtfeger, P.D.W. Boyd, G.A. Bowmaker, H.G. Mack, H. Oberhammer, Theoretical studies on the stability of thallium-carbon. sigma.-bonds in aliphatic organothallium compounds, J. Am. Chem. Soc. 111 (1) (1989) 15–23.
[70] E.M. Spain, M.D. Morse, Bond strengths of transition-metal dimers: titanium-vanadium (TiV), vanadium dimer, titanium-cobalt (TiCo), and vanadium-nickel (VNi), J. Phys. Chem. 96 (6) (1992) 2479–2486.
[71] M.B. Knickelbein, S. Yang, Photoionization studies of niobium clusters: ionization potentials for Nb2–Nb76, J. Chem. Phys. 93 (8) (1990) 5760–5767.
[72] A.C. Borin, J.P. Gobbo, Electronic structure and chemical bonding in the ground and low-lying electronic states of Ta2, Int. J. Quantum Chem. 111 (7–8) (2011) 1306–1315.
[73] P.A. Christiansen, W.C. Ermler, K.S. Pitzer, Relativistic effects in chemical systems, Annu. Rev. Phys. Chem. 36 (1) (1985) 407–432.
[74] P. Schwerdtfeger, Relativistic effects in properties of gold, Heteroat. Chem. 13 (6) (2002) 578–584.
[75] M. Bardají, A. Laguna, Gold chemistry: the aurophilic attraction, J. Chem. Educ. 76 (2) (1999) 201.
[76] H. Schmidbaur, The aurophilicity phenomenon: a decade of experimental findings, theoretical concepts and emerging applications, Gold Bull. 33 (1) (2000) 3–10.
[77] Z.H. Li, D.G. Truhlar, Nanothermodynamics of metal nanoparticles, Chem. Sci. 5 (7) (2014) 2605–2624.
[78] W.D. Knight, K. Clemenger, W.A. de Heer, W.A. Saunders, M.Y. Chou, M.L. Cohen, Electronic shell structure and abundances of sodium clusters, Phys. Rev. Lett. 52 (24) (1984) 2141.
[79] K. Clemenger, Ellipsoidal shell structure in free-electron metal clusters, Phys. Rev. B 32 (2) (1995) 1359.
[80] W.G. Sun, J.J. Wang, C. Lu, X.X. Xia, X.Y. Kuang, A. Hermann, Evolution of the structural and electronic properties of medium-sized sodium clusters: a honeycomb-like Na_{20} cluster, Inorg. Chem. 56 (3) (2017) 1241–1248.
[81] T. Höltzl, T. Veszprémi, P. Lievensc, M.T. Nguyen, Aromaticity and Metal Clusters, CRC Press, Boca Raton, FL, 2010.
[82] C.G. Li, Z.G. Shen, Y.F. Hu, Y.N. Tang, W.G. Chen, B.Z. Ren, Insights into the structures and electronic properties of Cu_{n+1}^{μ} and Cu_nS^{μ} (n = 1–12; μ = 0,±1) clusters, Sci. Rep. 7 (1) (2017) 1–11.
[83] T. Holtzl, P. Lievens, T. Veszprémi, M.T. Nguyen, Comment on "Tuning magnetic moments by 3d transition-metal-doped Au_6 clusters", J. Phys. Chem. C 113 (49) (2009) 21016–21018.
[84] M.P. Johansson, P. Pyykkö, The importance of being tetrahedral: the cadmium pyramids Cd_N; N = 4, 10, 20, 35 and 56, Phys. Chem. Chem. Phys. 6 (11) (2004) 2907–2909.
[85] K.A. Jackson, First-principles study of the structural and electronic properties of Cu clusters, Phys. Rev. B 47 (15) (1993) 9715.
[86] S. Lecoultre, A. Rydlo, C. Félix, J. Buttet, S. Gilb, W. Harbich, UV–visible absorption of small gold clusters in neon: Au_n (n = 1–5 and 7–9), J. Chem. Phys. 134 (7) (2011), 074302.

[87] S.M. Morton, D.W. Silverstein, L. Jensen, Theoretical studies of plasmonics using electronic structure methods, Chem. Rev. 111 (6) (2011) 3962–3994.
[88] N. Durante, A. Fortunelli, M. Broyer, M. Stener, Optical properties of Au nanoclusters from TD-DFT calculations, J. Phys. Chem. C 115 (14) (2011) 6277–6282.
[89] J.V. Koppen, M. Hapka, M.M. Szczęśniak, G. Chałasiński, Optical absorption spectra of gold clusters Au_n (n = 4, 6, 8, 12, 20) from long-range corrected functionals with optimal tuning, J. Chem. Phys. 137 (11) (2012), 114302.
[90] S. Lecoultre, A. Rydlo, J. Buttet, C. Félix, S. Gilb, W. Harbich, Ultraviolet-visible absorption of small silver clusters in neon: Ag_n (n = 1–9), J. Chem. Phys. 134 (18) (2011), 184504.
[91] G.A. Bishea, M.D. Morse, Spectroscopic studies of jet-cooled AgAu and Au2, J. Chem. Phys. 95 (8) (1991) 5646–5659.
[92] S. Fedrigo, W. Harbich, J. Buttet, Optical response of Ag_2, Ag_3, Au_2, and Au_3 in argon matrices, J. Chem. Phys. 99 (8) (1993) 5712–5717.
[93] H. Häkkinen, B. Yoon, U. Landman, X. Li, H.-J. Zhai, L.-S. Wang, On the elctronic and atomic structures of small Au_N^- (N = 4 − 14) Clusters: a photoelectron spectroscopy and density-functional study, J. Phys. Chem. A 107 (32) (2003) 6168–6175.
[94] B. Collings, K. Athanassenas, D. Lacombe, D. Rayner, P. Hackett, Optical absorption spectra of Au_7, Au_9, Au_{11}, and Au_{13}, and their cations: gold clusters with 6, 7, 8, 9, 10, 11, 12, and 13 s-electrons, J. Chem. Phys. 101 (5) (1994) 3506–3513.
[95] B. Anak, M. Bencharif, F. Rabilloud, Time-dependent density functional study of UV-visible absorption spectra of small noble metal clusters (Cu_n, Ag_n, Au_n, n = 2–9, 20), RSC Adv. 4 (25) (2014) 13001–13011.
[96] A. Castro, M.A. Marques, A.H. Romero, M.J. Oliveira, A. Rubio, The role of dimensionality on the quenching of spin-orbit effects in the optics of gold nanostructures, J. Chem. Phys. 129 (14) (2008), 144110.
[97] C.M. Aikens, G.C. Schatz, TDDFT studies of absorption and SERS spectra of pyridine interacting with Au_{20}, J. Phys. Chem. A 110 (49) (2006) 13317–13324.
[98] R.B. Wyrwas, M.M. Alvarez, J.T. Khoury, R.C. Price, T.G. Schaaff, R.L. Whetten, The colours of nanometric gold, Eur. Phys. J. D 43 (1) (2007) 91–95.
[99] M. Zhu, C.M. Aikens, F.J. Hollander, G.C. Schatz, R. Jin, Correlating the crystal structure of a thiol-protected Au_{25} cluster and optical properties, J. Am. Chem. Soc. 130 (18) (2008) 5883–5885.
[100] S. Mitchell, J. Farrell, G. Kenney-Wallace, G. Ozin, Optical emission and absorption studies of silver atoms in rare gas matrixes at 12 K; silver atom cryophotoaggregation, J. Am. Chem. Soc. 102 (26) (1980) 7702–7709.
[101] W. Li, F. Chen, Structural, electronic and optical properties of 7-atom Ag-Cu nanoclusters from density functional theory, Eur. Phys. J. D 68 (4) (2014) 1–11.
[102] N.T. Cuong, N.T.M. Hue, N.M. Tho, Theoretical modeling of optical properties of Ag_8 and Ag_{14} silver clusters embedded in an LTA sodalite zeolite cavity, Phys. Chem. Chem. Phys. 15 (2013) 15404–15415.
[103] W. Harbich, Y. Belyaev, R. Kleiber, J. Buttet, Optical spectroscopy of size-selected silver clusters embedded in solid neon: a cluster-support interaction study, Surf. Rev. Lett. 3 (01) (1996) 1147–1152.
[104] F. Conus, V. Rodrigues, S. Lecoultre, A. Rydlo, C. Félix, Matrix effects on the optical response of silver nanoclusters, J. Chem. Phys. 125 (2) (2006), 024511.
[105] J.C. Idrobo, S. Öğüt, K. Nemeth, J. Jellinek, R. Ferrando, First-principles isomer-specific absorption spectra of Ag_{11}, Phys. Rev. B 75 (23) (2007), 233411.
[106] S. Fedrigo, W. Harbich, J. Buttet, Collective dipole oscillations in small silver clusters embedded in rare-gas matrices, Phys. Rev. B 47 (16) (1993) 10706.
[107] F. Rabilloud, UV-visible absorption spectra of metallic clusters from TDDFT calculations, Eur. Phys. J. D 67 (2013) 18.